SCUOLA DI SCIENZE
Dipartimento di Chimica Industriale “Toso Montanari”

Corso di Laurea Magistrale in

Chimica Industriale

Classe LM-71 - Scienze e Tecnologie della Chimica Industriale

Low temperature hydrodeoxygenation of vanillin: unlocking bimetallic synergy

Tesi di laurea sperimentale

CANDIDATO

Simone Govoni

RELATORE

Chiar.mo Prof. Nikolaos Dimitratos

CORRELATORE

Dr Robert Wojcieszak

Anno Accademico 2022-2023

INDEX

1 INTRODUCTION

The global energy landscape today stands at a critical juncture, marked by an ever-increasing demand for energy driven by population growth, industrialization, and the pursuit of higher living standards across the globe. This surge in energy demand has historically been met predominantly through the exploitation of fossil fuels (coal, oil, and natural gas) resources that have powered the world's economies for over a century. However, the reliance on these carbon-intensive energy sources has precipitated a host of environmental, economic, and social challenges, casting a long shadow on the sustainability of global energy practices. The environmental impact of fossil fuel consumption is both profound and far-reaching. The combustion of these resources is the largest contributor to carbon dioxide emissions, a potent greenhouse gas that is the primary driver of global climate change. The repercussions of climate change are manifold, ranging from extreme weather events and rising sea levels to the disruption of ecosystems and agriculture [1]. In this context, renewable energy sources, such as solar, wind, hydro, and biomass, emerge as pivotal elements in the quest for sustainable energy solutions. Unlike fossil fuels, renewables offer a virtually inexhaustible supply of energy, with minimal direct emissions of greenhouse gases or pollutants. The harnessing of renewable energy thus stands as a cornerstone in the global strategy to mitigate climate change, promising to reduce the carbon intensity of energy systems and foster environmental stewardship. Beyond environmental benefits, the transition to renewable energy also holds the promise of enhancing energy security. By diversifying the energy mix and reducing dependence on imported fuels, countries can shield themselves from the volatility of global energy markets and the geopolitical tensions that often accompany the scramble for fossil fuel resources. However, the transition to renewable energy is fraught with challenges. Technological and economic barriers remain significant hurdles to the widespread adoption of renewable energy technologies. Many renewable energy sources are intermittent in nature, as solar and wind energy, and necessitating advances in energy storage and grid management to ensure reliability and stability of supply. These challenges in renewable energy use have led to a continuous increase in petroleum-based energy consumption (Figure 1 [2]). This situation underscores the urgent need for alternative energy sources.

Biomass emerging as a promising candidate due to its potential for conversion into liquid fuels and chemicals, thereby offering a sustainable and green alternative to conventional fossil fuel-based energy and chemical sources.

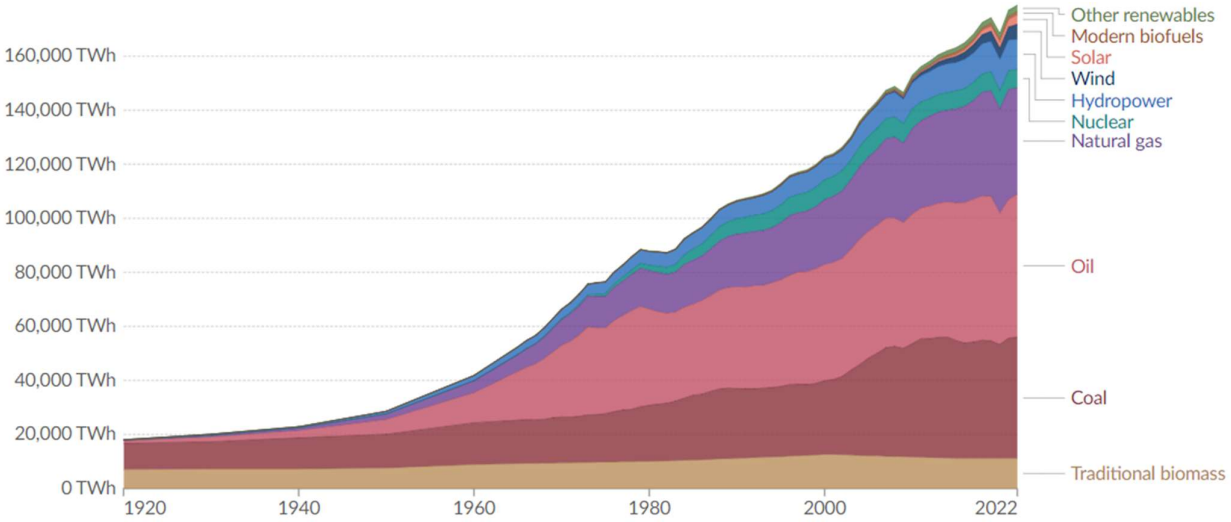

Figure 1. World energy consumption through the years divided per source [2].

2 BIOMASS

The transition towards renewable energy sources necessitates a critical evaluation of biomass as a resource for biofuels and biochemicals (Figure 2 [3]). Biomass can be categorized into two types: first-generation and second-generation biomass. First-generation biomass primarily encompasses organic materials derived directly from food crops. These include sugarcane, corn, and vegetable oils, which are directly processed to produce bioethanol and biodiesel. The use of first-generation biomass is often criticized due to the competition it creates with food supplies and the consequent implications for food security and prices. Furthermore, these biomass resources are limited by the arable land available, thus capping their potential for renewable energy production. In contrast, second-generation biomass refers to non-food biomass, woody crops, agricultural residues, energy crops, waste streams: more general term, lignocellulosic biomass. This type of biomass does not compete directly with food resources and has a lower environmental impact. Through thermal and chemical

processes, lignocellulosic biomass, can be converted into a range of biofuels and chemicals. These technologies enable the utilization of a wider array of biomass sources, including those that are not suitable for human consumption, expanding the potential for sustainable and scalable bioenergy production.

As such, lignocellulosic biomass stands at the forefront of innovative solutions in the renewable energy sector, representing a critical step towards an environmentally and economically balanced energy future.

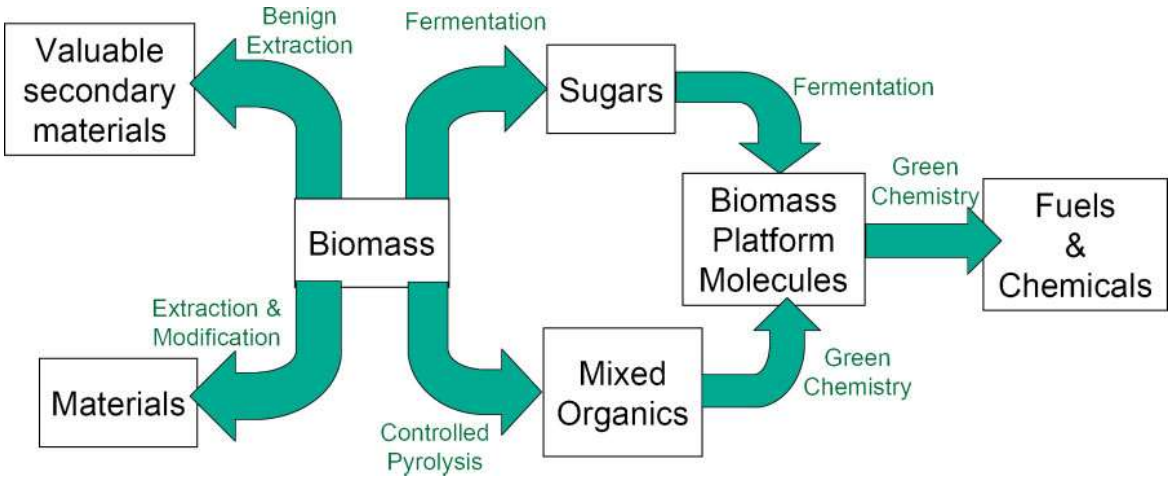

Figure 2. Possibilities in biomass conversion [3].

Lignocellulosic biomass conversion faces different challenges than petroleum refining. As opposed to the relatively generic and composition-consistent oil, lignocellulosic biomass varies greatly from species to species and from season to season; one requirement of a biorefinery is that it is able to cope with altering feedstock composition. Unlike petroleum, biomass experiences seasonal changes; harvesting is not possible throughout the entire year. A switch from crude oil to biomass may require a change in the capacity of chemical industries, with a requirement to generate the materials and chemicals in a seasonal timeframe.

Over the years, numerous processes have been studied and developed to convert lignocellulosic biomass effectively and efficiently, these conversion techniques can be categorized into three main groups:

- thermal conversion: involves the conversion of organic materials primarily harnessing the heat content of the biomasses.
- chemical conversion: conversion of biomass through biochemical pathways or chemical processes
- thermochemical: a combination of the two previous.

2.1 Thermal conversion of lignocellulosic biomass

The thermal breakdown of biomass can occur in various forms, including drying, combustion, torrefaction, carbonization, gasification, and pyrolysis, contingent upon the temperature and oxygen levels involved in the process [4]:

- Hydrothermal Carbonization (HTC): operates at 180-250 °C using hot pressurized water, transforming biomass into hydrochar, along with gaseous and liquid residues. HTC offers a sustainable way to produce solid fuel but requires energy for high-pressure maintenance.
- Combustion**:** burns biomass in the presence of oxygen to produce thermal energy and flue gas. While it's the most straightforward method for energy extraction from biomass, it's less environmentally friendly due to potential emissions and the loss of valuable biomass components.
- Torrefaction**:** occurs at 200-300 °C reducing biomass to 70% of its original mass while increasing its energy density. The process improves biomass's physical and chemical properties, making it easier to grind and hydrophobic, although it results in a 30% loss through gas and volatile matter release.
- Gasification: biomass is subjected to a limited oxygen supply at 800-1000°C, producing a syngas composed of CO and H_2. This process allows for the efficient production of a versatile fuel gas but requires careful control of operating conditions to optimize syngas composition.
- Slow Pyrolysis: at 280-550 °C, mainly produces biochar from biomass, along with tar and other gases. It's beneficial for producing solid fuel and sequestering carbon but is less efficient in converting biomass to liquid or gas fuels.
- Fast Pyrolysis**:** heats biomass rapidly to 500-800 °C, yielding biochar, bio-oil, and flammable gas. This process is efficient for producing bio-oil but requires rapid heating and cooling, which can be energy-intensive.

Each of these processes offers unique benefits in terms of the products they yield and their potential applications, from energy production to the creation of value-added chemicals and materials. In Figure 3 is reported a graphic that summarizes the thermal conversions. In the x-axes, the "Φ" is an oxygen factor, indicative on the amount of oxygen consumed for each technique [4].

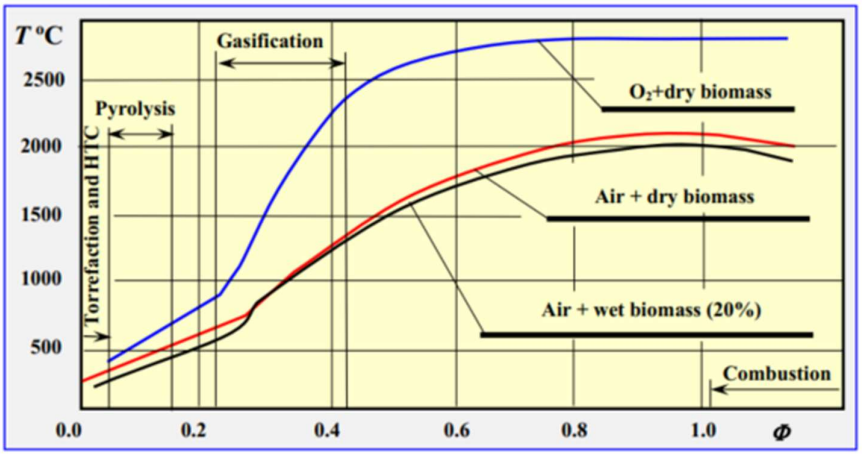

Figure 3. Oxygen consumed at temperature conditions at which occurs the different type of thermal conversion.

2.2 Lignocellulosic biomass composition

To comprehend how the lignocellulosic biomass could be converted into fuel and useful chemicals, is important to understand its chemical characteristics itself, and what are the features that make this a powerful resource. Thus, in this chapter it will be reported the three major components that constitute the lignocellulosic biomass: cellulose, hemicellulose, and lignin.

2.2.1 Cellulose

Cellulose a homopolymer composed exclusively of glucose units linked by β-1,4-glycosidic bonds (Figure 4). Its highly ordered structure leads to the formation of microfibrils, which exhibit considerable tensile strength. These microfibrils are essentially crystalline regions where the chains of glucose molecules are tightly packed and hydrogen-bonded together, resulting in fibers of high tensile strength and insolubility. This organized structure makes cellulose resistant to hydrolysis and

digestion by most microorganisms and enzymes, except for specialized cellulase enzymes. The durability of cellulose is a contributing factor to its diverse applications, ranging from the production of paper and textiles to its use as a feedstock for biofuels and in the creation of biodegradable plastics and other materials.

2.2.2 Hemicellulose

Hemicellulose, in contrast to cellulose, is a heteropolymer and additionally the structure of the hemicellulose varies depending on the source of the lignocellulose, that may consist of various sugar monomers including glucose, xylose, mannose, galactose, rhamnose, and arabinose, among others. Hemicellulose has a branched structure with β-1,4-linked backbones and various side chains, making them amorphous and less crystalline compared to cellulose [5]. This structure renders hemicellulose more soluble in water and more easily hydrolyzable by acids, bases, and a range of hemicellulase enzymes, a useful feature in order to use this part of the lignocellulosic biomass as starting reagent for chemical transformations. Hemicelluloses serve as a filler in the cell wall, linking cellulose fibers and lignin, another cell wall component, to form a complex matrix that imparts flexibility to the plant structure [6].

2.2.3 Lignin

Lignin, an amorphous polymer, varies in structure depending on its biomass source and accounts for 15-30% of lignocellulosic biomass by weight. It is distinguished by a high content of aromatic groups and comprises three main monomers: p-coumaryl alcohol, coniferyl alcohol, and sinapyl alcohol (Figure 4 [6]). Lignin, with its unique structure and chemical makeup, holds great promise for generating a wide variety of common and specialized chemicals, particularly aromatic compounds and fuels. This positions it as a key source of aromatic resources for a bio-based economy. Traditionally, in industries like paper production and biorefineries that process wood, lignin was often viewed as a by-product rather than a valuable material, with its removal leading to difficult-to-manage solid waste. It was primarily burned as a basic form of solid fuel. However, converting lignin into useful chemicals and fuels, especially by utilizing its monomeric components, presents a substantial opportunity to tap into roughly 40% of the energy stored in biomass due to its high carbon content [7]. Being the richest natural

source of aromatic compounds, which are mainly sourced from petroleum in current industrial practices, it's crucial to develop efficient methods to harness this natural resource.

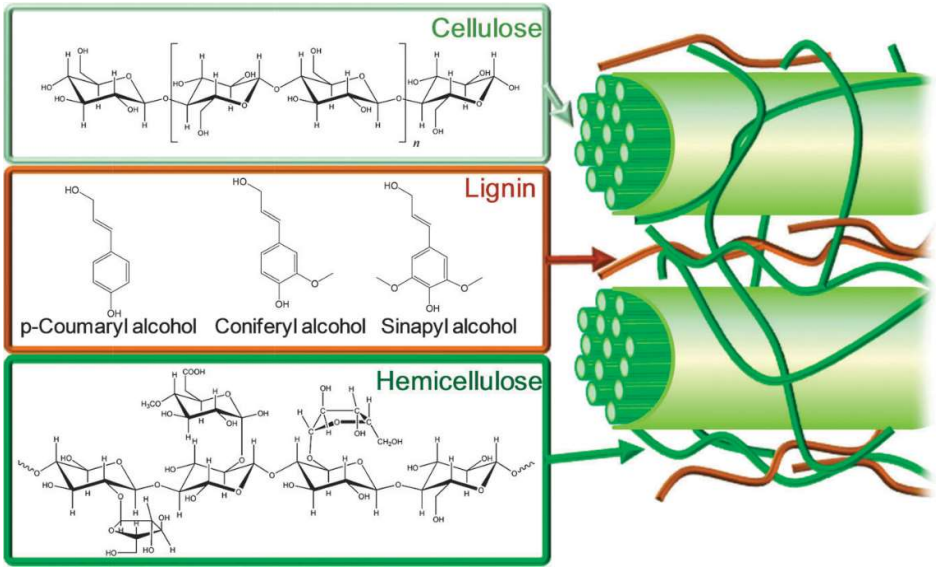

Figure 4. Composition of lignocellulosic biomass.

2.3 Lignocellulosic biomass chemical conversion strategies

To use a single lignocellulosic fraction as starting molecule it is necessary the extraction and individual processing of each one of them. This is facilitated by chemical, thermal, and microbiological methods, including ammonia fiber explosion, chemical treatment, biological treatment and steam explosion, leveraging their distinct structures and compositions [8–10]. This approach enables the customized production of various chemical products and fuels by adjusting the reaction conditions tailored to each specific component. Each technique can be more or less specialized in extracting or deselecting a particular fraction of cellulosic biomass. For instance, treatment with strong acids can dissolve hemicellulose without affecting cellulose, making the latter less crystalline, more porous, and thereby more accessible to hydrolytic enzymes.

2.3.1 Cellulosic biomass valorisation

Cellulosic biomass, cellulose and hemicellulose, has been intensively studied in the past as a promising and sustainable source of sugars for various bio-based products,

including bioethanol. Due to the structure of the cellulosic biomass, the emphasis has been on converting cellulose and hemicellulose into fermentable sugars. The conversion of this biomass into sugars has been confirmed as a viable and sustainable pathway to produce bio-alcohol and other biochemicals.

One of the earliest applications of cellulosic biomass is the production of bioethanol. The process of generating bioethanol from cellulosic biomass is intricate, encompassing several stages, commencing with pretreatment to hydrolyse biomass into fermentable sugars, succeeded by microbial fermentation to transform these sugars into ethanol. Recent advancements highlight the optimization of pretreatment processes and enzymatic hydrolysis to enhance the yield and efficiency of bioethanol production. For instance, acidic and alkaline pretreatments have been shown to effectively degrade hemicelluloses and lignin, respectively, improving cellulose accessibility for subsequent enzymatic conversion to glucose [11].

In the literature, it is well-documented that various chemicals can be ideally synthesized from these sugars through enzymatic or chemo-catalytic processes, including: hydrogenation to C5-C6 polyols, hydrogenolysis to C2-C3 glycols, oxidation, halogenation, dehydration, carbon-carbon (C-C) coupling and deoxygenation. Examples of sugar-derived building blocks include 1,4-diacids (such as succinic, fumaric, and malic acids), 2,5-furan dicarboxylic acid (FDCA), 3-hydroxypropionic acid, and levulinic acid. [12] These compounds are essential for the synthesis of a wide array of bio-based products, highlighting the immense potential of biomass as a renewable resource [13]. They play a critical role in the manufacture of bio-based polyesters, platform chemicals, acids, intermediates for further synthesis, and biodegradable plastics. For instance, FDCA is recognized as a promising alternative to terephthalic acid in the production of polyesters, while succinic and levulinic acids are key precursors for a variety of valuable bio-products, including bioplastics and solvents. Scholarly research emphasizes the efficiency and sustainability of employing these sugar-derived compounds to produce eco-friendly materials and chemicals, thus significantly propelling forward the domains of green chemistry and the bioeconomy [12].

2.3.2 Lignin valorisation

While the transformation of cellulosic biomass has been closely examined, interest in converting lignin into useful products has significantly increased just in the last two decades, driven by the goal to make the most of lignocellulosic biomass. This change is due to the understanding that focusing only on cellulose and hemicellulose turns lignin into an overlooked by-product, despite it being a rich source of valuable phenolic compounds. These compounds are now recognized for their importance in producing fuels and chemicals, encouraging a more inclusive approach to biomass conversion [14]. However, the tough nature of lignin makes it difficult to use and convert through chemical or enzymatic methods.

In contrast to the selective breakdown of biomass components and meeting the desire to include also lignin in feasible valorisation processes, methods like gasification or pyrolysis offer a less selective, yet simpler, approach to converting the entire biomass, emphasizing the strategic balance between process simplicity and molecular selectivity [15,16]. This approach underscores the importance of developing methodologies that capture the full value of lignocellulosic biomass for the renewable energy and chemical manufacturing industries, emphasizing its critical role in fostering sustainable technologies. Addressing the high oxygenation and functionality of biomass is essential for increasing energy density in fuel applications and for achieving high yields of valuable chemicals through selective reactivity reduction. A compact resuming scheme of the various possible pathways in the valorisation of biomass is presented in Figure 5 [17].

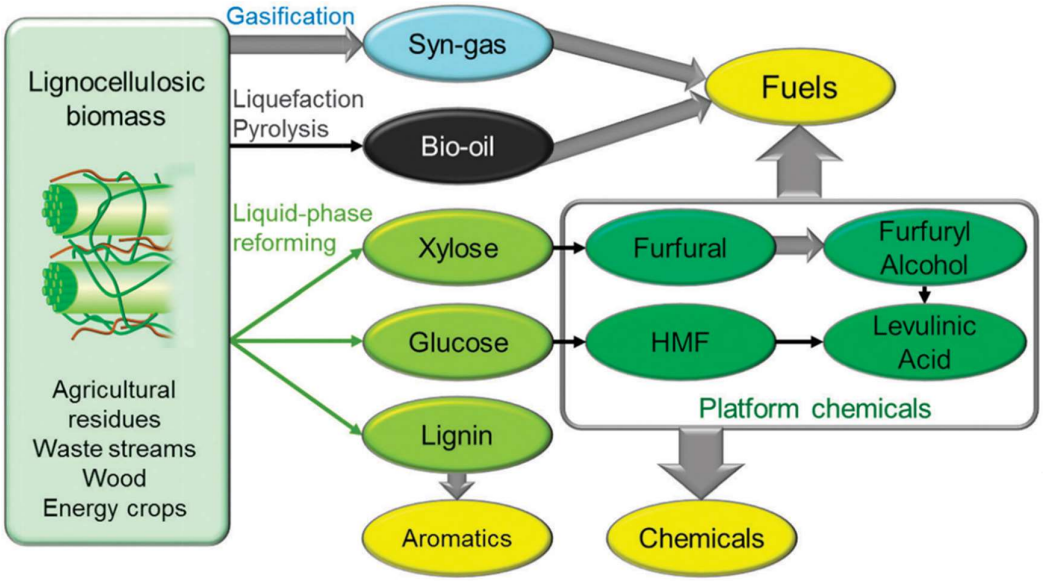

Figure 5. Resuming scheme of different valorisation pathways for lignocellulosic biomass [17].

2.4 BIO-OIL

In past years the role of fast pyrolysis as a pivotal thermal conversion technology for biomass upgrading has been object of much research [18]. The interest on this technique risen because it offers a promising pathway for transforming lignocellulosic biomass into valuable liquid fuels and chemical feedstocks. This process involves the rapid heating of biomass to moderate temperatures (typically around 500 °C) in the absence of oxygen, followed by the swift cooling of the resulting vapours to yield bio-oil, along with char and gas by-products. The primary appeal of fast pyrolysis lies in its ability to achieve high yields of bio-oil. The efficiency and outcome of fast pyrolysis are significantly influenced by various operational parameters, including the pyrolysis temperature, heating rate, residence time, and biomass particle size. The resulting bio-oil, under optimized conditions, can constitute up to 75% of the starting biomass by weight [19].

2.4.1 Bio-oil characteristics

Pyrolytic bio-oil is produced from the thermal decomposition of biomass constituents such as cellulose, hemicellulose, and lignin. It's markedly different from conventional crude oil, given its composition of over 300 oxygenated compounds, including diverse organic molecules like acids, alcohols, ketones, and esters. Notably, phenolic

compounds such as phenol and guaiacol originate from lignin, while the depolymerization of cellulose and hemicellulose gives rise to sugars and furans[20]. The physical and chemical properties of bio-oil are significantly influenced by its high oxygen content and lower hydrogen-to-carbon ratio, resulting in a lower heating value and high acidity, which also contributes to its incompatibility with hydrocarbon fuels (Figure 6). Undesirable features of bio-oil like thermal instability, seen in increased viscosity over time, and its corrosiveness, pose challenges for storage and use. Furthermore, condensation and polymerization reactions can lead to the formation of heavier, coke-like residues during distillation. For bio-oil to become a feasible substitute for petroleum fuels and to serve as a feedstock in the chemical industry, it requires upgrading to remove the excessive oxygenated functionalities. This enhancement is essential to align its properties with those needed for industrial applications, allowing bio-oil to emerge as a sustainable alternative to fossil fuels in various chemical and energy-related uses.

	Bio-oil	Crude oil
water (%)	15-30	0.1
pH	2.8-3.8	-
ρ (kg/L)	1.05-1.25	0.86
μ50°C (cP)	40-100	180
HHV (MJ/KG)	16-19	44
C (%)	55-65	83-86
O (%)	28-40	< 1
H (%)	5-7	11-14
S (%)	< 0.05	< 4
N (%)	<0.4	< 1
ash (%)	< 0.2	< 0.1

Figure 6. Differences between bio-oil and crude oil.

2.4.2 Upgrade paths of bio-oil

In order to overcome the deleterious properties of the biomass pyrolysis oil, the upgrading process is required before its application. In the years, many studies were done to find method designed to enhance the property of bio-oil, as:

- **Esterification and Emulsification**: Esterification involves reacting bio-oil components with alcohols to form esters, reducing acidity and improving stability. This process can be combined with emulsification, where bio-oil is blended with conventional fuels to improve compatibility with existing fuel systems[21].
- **Supercritical Fluid Treatment**: Upgrading bio-oil in supercritical fluids, such as ethanol and water, has been explored as a non-catalytic method. This process can lead to the depolymerization of large molecules and reduction of oxygen content through solvent effects and thermal cracking. The use of supercritical ethanol has shown to enhance the HHV (High Heating Value) of bio-oil and reduce its acidity and water content [22]
- **Co-pyrolysis**: Co-pyrolysis involves the pyrolysis of biomass with other materials, such as plastics or waste oils, in the presence of catalysts. This method can synergistically improve the yield and quality of bio-oil by incorporating hydrogen-rich feedstocks that contribute to the deoxygenation and stabilization of the resulting bio-oil [23]
- **Hydrodeoxygenation (HDO)**: HDO is a promising technique for bio-oil upgrading, involving the treatment of bio-oil in the presence of hydrogen over a suitable catalyst to remove oxygen as water. This process significantly improves the quality of bio-oil by increasing its calorific value and reducing acidity and viscosity [24]

These are some of the most utilized techniques. After treatment, the bio-oil thus becomes usable as a viable, renewable alternative to conventional petroleum products in various chemical and energy applications.

2.4.3 Model molecules

Addressing the challenges of utilizing lignin and bio-oil as starting materials has led to the adoption of model molecules as a more manageable strategy for investigating their conversion processes. The inherent heterogeneity and complex structure of lignin have traditionally posed significant barriers to its efficient depolymerization and valorisation. Utilizing model compounds enables a more focused study of specific reactions and pathways, offering a controlled environment for unrevealing reaction mechanisms and

pinpointing the optimal conditions for catalytic processes, such as hydrodeoxygenation (HDO) [25].

This approach of breaking down the complex matrices of bio-oil and lignin into simpler, representative model compounds allows researchers to effectively explore and enhance the conversion processes needed to transform these materials into valuable products. The literature highlights a variety of model molecules that have been explored to optimize conversion processes. These model molecules aim to closely represent the complex phenolic structure of lignin and the compounds derivable from it in bio-oil. Molecules featuring aromatic rings and oxygenated functional groups have been targeted for investigating the reactivity in HDO reactions, among other techniques. Figures 7 and 8 [26] show some of the model molecules employed for this purpose in contraposition to the lignin monomers.

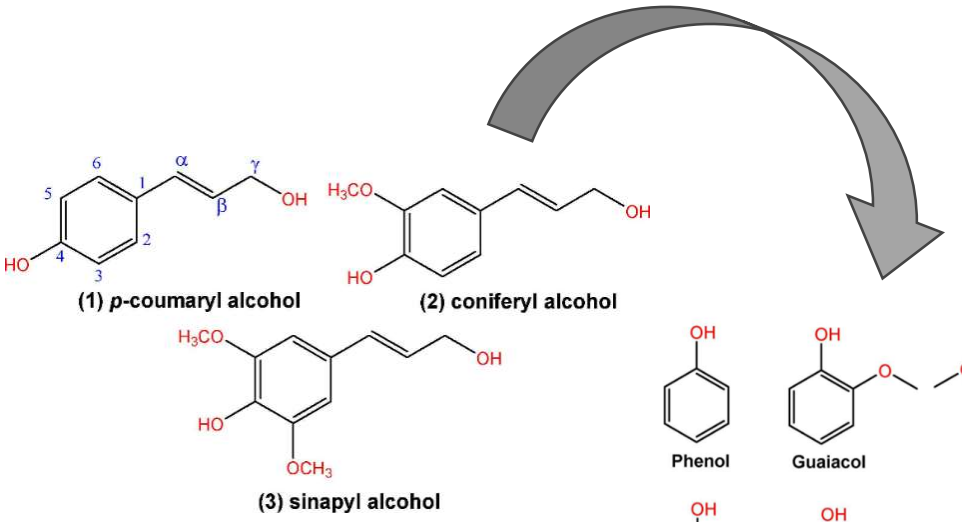

Figure 7. The three primary types of alcohols in lignin.

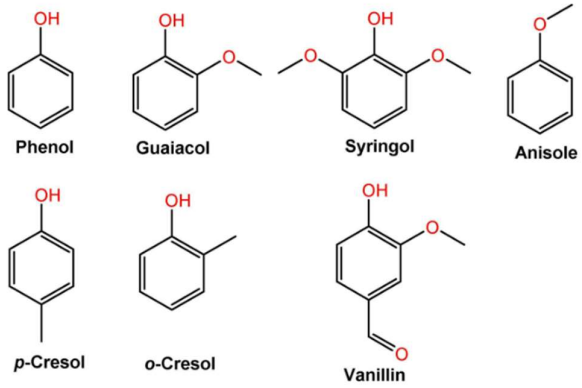

Figure 8. More common model molecules used.

3 HYDRODEOXIGENATION (HDO)

3.1 Chemistry of HDO

Between the biomass valorisation technique, hydrodeoxygenation (HDO) is a crucial process and the most extensively researched for converting lignocellulosic biomass into valuable hydrocarbons, marking a vital step towards the production of drop-in biofuels and high-value, bio-derived chemicals. HDO involves the catalytic removal of oxygen from biomass-derived oxygenates.

The HDO reaction, a form of hydrogenolysis, is aimed at eliminating oxygen from oxygenated compounds, simplistic represented by the reaction:

$$R_2O + 2H_2 \rightarrow H_2O + 2\,RH$$

The reaction is more complex than this. In their recent work, Wang et al. (2020) [27] indicated the reaction path of HDO, using phenol as an example, a very common model molecule for bio-oil (Figure 9).

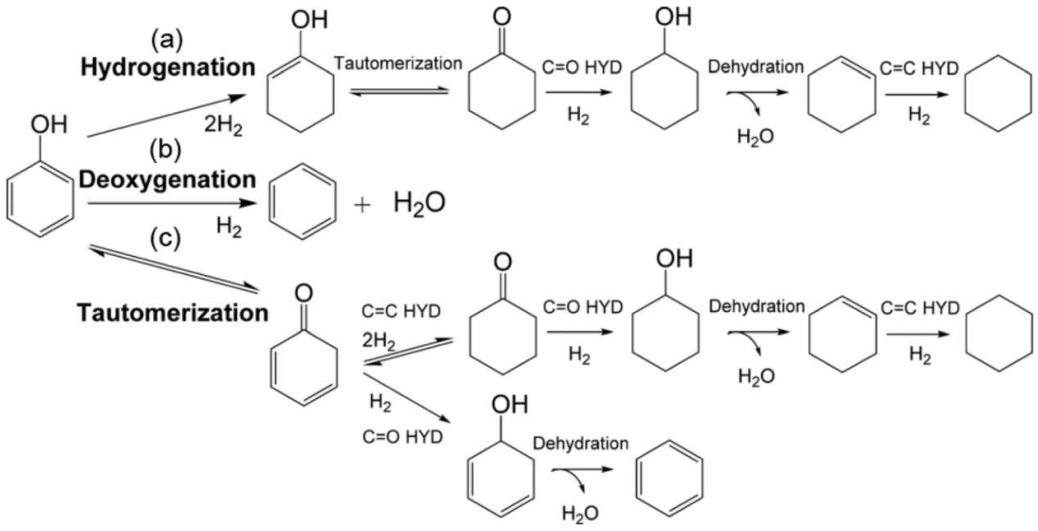

Figure 9. Different typical routes in HDO of phenol.

Hydrogenation Pathway (a): This process begins with the partial hydrogenation of the aromatic ring to form cyclohexanone, which is then further hydrogenated to

cyclohexanol. This reaction sequence happens swiftly, preventing the buildup of cyclohexanone. The slowest step in this pathway is the conversion of cyclohexanol to cyclohexene, due to the breaking of the C–O bond, culminating in the production of cyclohexane as the final product without oxygen. Direct Deoxygenation Pathway (b): Offers a simpler, more hydrogen-efficient method that produces benzene as the final product. However, this pathway faces challenges due to the stronger C–O bond in phenol compared to that in cyclohexanol, making the bond dissociation more difficult. Tautomerization Pathway (c): Involves creating a keto intermediate (2,4-cyclohexadienone), which may either undergo hydrogenation leading to ring saturation, similar to pathway (a), or proceed through reactions characteristic of direct deoxygenation if the carbonyl group is hydrogenated.

This reveals that the reaction pathways for lignin/bio-oil model molecules, due to their high level of functionalization and the typically highly reactive catalysts used, present numerous reaction opportunities under the standard conditions in which HDOs are typically performed.

HDO of lignin-derived phenolics is usually operated at high reaction temperatures (200–400 °C) in the presence of H donors such as hydrogen (externally supplied or generated in situ) and a suitable solvent. HDO has been intensively investigated in the presence of gaseous H_2 at pressures from atmospheric pressure to 20 MPa. As demonstrated in several studies, the hydrogen pressure tremendously influences the HDO processes: enhancing hydrogen pressure would promote HDO because more active H species are supplied, thus potentially altering the reaction pathway. However, the excessive hydrogenation of aromatic rings is unavoidable at high hydrogen pressures. Typically, the hydrogenation of the benzene ring is suppressed when a low hydrogen pressure (typically <1 MPa) is used. This is a crucial point on the development of this valorisation technique. The maintaining of the aromatic ring, in most of the cases, is a very tailored objective in the HDO of model molecules of lignin and bio-oil, because it preserves the high-value aromatic structure that are essential for the production of specific chemicals and fuels, such as phenolic resins, fine chemicals and fuel additives. Thus, the challenge that researchers are striving for, lies in selectively removing oxygen-containing functional groups without hydrogenating aromatic ring itself, which

would lead to a loss of these valuable compounds. For example, in a study [28] biochar-modifies with Ni-V bimetallic catalysts for the HDO of guaiacol were studied. It has been demonstrated that modifications could give enhancing selectivity towards aromatic hydrocarbons. Details of these results are reported in Table 2.

Table 2. Aromatic selectivity obtained varying modifications on catalyst system.

Catalyst Type	Aromatic Selectivity (%)
H_2/Ni-V + PB/Ni-V	36.71%
H_2/Ni-V	36.78%
PB-H_2-4/Ni-V	49.45%
PB-H_2-16/Ni-V	50.70%
PB-H_2-8/Ni-V	54.24%

By carefully selecting and optimizing the catalyst, it is possible to maximize the yield of valuable aromatic hydrocarbons, which are essential for the sustainable production of bio-based chemicals and fuels.

3.2 Catalyst selection in HDO reactions

The choice of the catalyst is a critical factor, significantly impacting for hydrodeoxygenation (HDO) of lignin or bio-oil model molecules due to the complex nature of these feedstocks and the diversity of chemical reactions involved in their conversion. Literature has documented a lot of types of catalyst that demonstrated to be highly efficient in the production of deoxygenated compounds.

3.2.1 Homogeneous vs Heterogeneous catalysis: a brief reminder

Both heterogeneous and homogeneous catalysis have been explored in HDO reactions, yet from an environmental perspective, heterogeneous catalysis has garnered more attention in research. It is well-known that, generally, heterogeneous catalysis, where the catalyst and substrate exist in separate phases, offers lower performance compared to its homogeneous counterpart. This difference is attributed to the fact that, in homogeneous catalysis, the catalyst is in the same phase as the substrate, allowing for

greater dispersion and thus more active sites exposed to the substrate. However, this often leads to significant challenges in separating the catalyst from the reaction mixture, potentially compromising material recovery and contaminating the final product with undesired by-products. Heterogeneous catalysis, on the other hand, provides the advantage of easy separation from the reaction mixture, enabling more efficient material recovery and offering the possibility of catalyst reuse in subsequent reactions. Therefore, is important evaluating the reusability of the catalyst, in the interest of sustainability and green chemistry,

The literature emphasizes the critical importance of catalyst design, with most of the heterogeneous catalysts explored for hydrodeoxygenation (HDO) being supported catalysts. In these, the active phase, which is the primary promoter of the reaction, is finely dispersed across the surfaces of a material known as the support. The effective integration of the support with the active sites is one of the key features that distinguish a heterogeneous catalyst, potentially leading to a material that exhibits superior catalytic performance.

3.2.2 Active phase

The active phase of the most extensively studied and utilized catalysts in hydrodeoxygenation (HDO) reaction research is typically metallic, which can be dispersed on the support surface in various forms, including nanoparticles, crystals, clusters, and single-atoms catalysts. Among these, nanoparticles are the most thoroughly investigated due to several advantages over other types of aggregations [29]:

- They are more stable and versatile across a wide range of catalytic applications compared to clusters and single-atom catalysts;
- They offer a greater specific surface area compared to crystals, enhancing their catalytic activity;
- Their electronic and geometric properties (and thus catalytic properties) can be easily adjusted by altering the size of the nanoparticles.

The metals most commonly used as active phases in the form of nanoparticles for HDO reaction catalysts include nickel (Ni), cobalt (Co), palladium (Pd), platinum (Pt), ruthenium (Ru), and molybdenum (Mo).

3.2.3 Support

The key characteristics that a catalyst support should possess can be broadly summarized as follows: (1) the ability to effectively interact with the active phase, enhancing its dispersion and thereby potentially reducing the amount of active phase needed, (2) a certain degree of porosity, as more porosity means greater surface area, providing more space for the active phase to reside, and (3) mechanical strength to withstand thermal and pressure stresses. The most commonly used supports in hydrodeoxygenation (HDO) reactions include:

- Metallic oxides, such as Al_2O_3, TiO_2, Nb_2O_5, SiO_2, MgO, ZrO_2, and their mixtures;
- Carbon-based supports, including activated carbon, carbon blacks, graphite, carbon nanotubes, and carbon nanofibers;
- Zeolites.

Therefore, the morphology of the support plays a crucial role in catalyst synthesis or usage, as it influences both the quantity and quality of accessible sites for the deposition of the active phase, as well as substrate accessibility. In the context of hydrodeoxygenation (HDO), the chemical nature of the support also becomes significantly important. A study [27] highlighted how the acidic nature of the support could, under certain conditions, facilitate the dissociation of the C-O bond. Specifically, when comparing the Pt/ZSM catalyst (a zeolite with strong acidity) and the Pt/Al_2O_3 catalyst (which has low acidity) in the HDO of guaiacol, the acidic support enabled the catalyst to achieve nearly 100% conversion of the substrate. In contrast, using Pt/Al_2O_3 under the same reaction conditions resulted in a 90% conversion.

A wide of different combinations of metals/supports have been studied in the past years. To provide an overview and context on the performance achieved over the years through the study of HDO on different model molecules, Table 3 succinctly summarizes the best outcomes obtained in some studies.

Table 3. Resume of some outcomes in HDO reactions in literature (a= creosol, b=phenol, c= cyclohexane, d= toluene, e= propylcyclohexane, f= cyclohexanol, h= oxygen-free aromatics)

Catalyst	Reagent	Time	T (°C)	P H_2 (bar)	Solvent	X (%)	S (%)	Ref.
Zn/Pd/C	Vanillin	8h	150	20	Methanol	>99	81[a]	[30]
Mo_2C/CNF	Guaiacol	4h	300	40	Dodecane	98	48[b]	[31]
Ni-SiO_2-ZrO_2	Guaiacol	8h	300	50	1-octanol	100	97[c]	[32]
CoNi/ Al_2O_3	Vanillin	1h	150	10	water	100	99[a]	[33]
Pt/alumina silicate	Guaiacol	1h	250	30	hexadecane	76	75[c]	[34]
MoO_3/ZrO_2	Anisole	1h	320	1	/	41	41[h]	[35]
Ni/SiO_2-ZrO	o-cresol	8h	300	50	/	100	93[d]	[36]
Pt/AC	4-propylphenol	1h	280	40	Water	100	97[e]	[37]
Ru/C	Phenol	1h	200	50	H_3PO_4– H_2O	100	88[c] 10[f] 1[g]	[34]

3.2.4 Bimetallic catalysts

The adoption of bimetallic catalysts, involving the combination of two metals on a support surface, is acknowledged in the scientific community as a promising avenue for enhancing biomass feedstock processing [28,38–44]. This synergistic metal interaction is capable of altering the surface attributes of the catalyst, which can lead to marked improvements in its performance. Specifically, these modifications can elevate the catalyst's activity, fine-tune its selectivity towards preferred outputs, and enhance its resilience against the impurities present in biomass-derived materials under more demanding reaction conditions. Utilizing bimetallic catalysts is considered a strategic approach, offering a broad spectrum of benefits. From a practical standpoint, the introduction of a secondary metal into the catalyst structure can significantly impact three key areas: (1) increased catalytic activity, (2) altered selectivity for targeted products, and (3) improved stability of the catalyst under operational conditions. Enhancement in catalysis can result from intricate interactions between metals, which can be categorized into five distinct phenomena:

- Geometric effects occur when the inclusion of a metal promoter changes the structure of the active sites made of the primary catalytic metal;
- Electronic effects involve the alteration of the electronic characteristics of the active sites, composed of the main catalytic metal, through electron sharing or transfer between the metals;
- Stabilizing effects describe how the presence of a metal promoter can enhance the durability of the catalytically active metal.
- Synergistic effects happen when both metal types contribute to the chemical bonding with reaction intermediates and transition states, improving the reaction process;
- Bi-functional effects refer to the scenario where each metal type fulfils a separate role within the overall reaction mechanism, leading to a more efficient catalytic process.

The inclusion of a second metal component adds complexity to the preparation of these materials, with the preparation method often dictating the final structure and, consequently, the properties of the materials. Thus, selecting the appropriate synthesis technique is vital for achieving a bimetallic material with the intended structure and desired properties. Techniques such as impregnation, co-precipitation, and deposition-precipitation have been employed to prepare bimetallic catalysts with controlled nanostructures, such as core-shell, alloy, or mixed metal oxides.

In the work [45] it is detailed how the two metals nanoparticles possible arrangements (Figure 10) influence various aspects of catalytic performance, including activity, selectivity, and stability, across different reactions. For instance, the presence of alloy phases between metals such as Sn and Pt is crucial for obtaining high activity in certain reactions, indicating that the structural arrangement of bimetallic particles plays a key role in catalytic processes. Additionally, research showed that changing the preparation techniques of the catalyst doesn't really affect how well it works. This suggests that what most influences the catalyst's performance is how the metals inside it interact with each other, rather than how the catalyst is made..

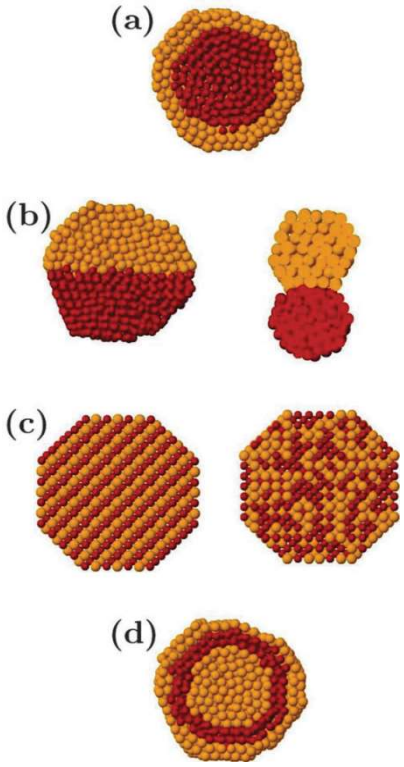

Figure 10. Different type of nanoparticles arrangements in bimetallic catalysts.

Although the bimetallic approach has been explored to a lesser extent than monometallic catalysts, its superior efficiency is well established in the literature. For instance, research highlighted in the work of Ardiyanti et al. (2012) [46] demonstrated that adding copper to a nickel/alumina catalyst significantly enhanced the hydrodeoxygenation (HDO) of fast pyrolysis oil compared to using a single-metal

catalyst. Specifically, the study reported a conversion rate of 79.6% with the bimetallic catalyst, versus 66.1% with the monometallic alternative, and an increase in the yield of oxygen-free products to 75.4% for the bimetallic, compared to 64.6% for the monometallic catalyst.

These results highlight the advantages of the bimetallic catalyst over the monometallic one in the HDO of bio-oil, suggesting that synergistic effect has occurred. New bimetallic catalysts need to be optimized specifically for each reaction ensuring high reaction rates, high selectivity, and yields that lead to effective purification steps.

4 OBJECTIVE OF THE THESIS AND SCIENTIFIC APPROACH

4.1 Scope of this work

In the study of converting lignin and bio-oil model molecules into useful products through hydrodeoxygenation (HDO), in the literature has been a significant emphasis on the study of monometallic catalytic systems. This preference is also due to the simpler way these single-metal systems can be understood and optimized, as they are less complex than systems using two metals. Yet, this has meant that bimetallic systems have not been as deeply explored, even though they might offer significant benefits for HDO processes.

Against this backdrop and building on the discussions in previous chapter regarding the valorisation of lignocellulosic biomass, this thesis main objective is to delve into the application of bimetallic catalytic systems in the HDO of representative lignin and bio-oil model molecules. A key question is whether using a simple and straightforward catalyst synthesis method like sol immobilization can actually lead to a situation where the two metals work better together, and how the ratio between these metals influences the catalyst's overall catalytic efficiency.

4.2 Choosing the Model Molecule

As explained in the previous chapter, model molecules are extremely valuable because they allow research efforts to focus primarily on exploring materials and their responses to reaction conditions, without the complexities associated with direct use of bio-oils or lignin, which have been previously discussed. This research began with two key decisions: the choice of the model molecule and the type of catalyst.

In selecting a model molecule, it is important to consider the basic structure of lignin, which contains phenolic and oxygenated groups. Among the model molecules, vanillin was chosen for its chemical structure. Vanillin, with its aromatic structure and three different oxygenated functional groups, emerges as a crucial molecule for understanding the chemical intricacies of lignin and bio-oil in HDO processes. The reaction pathway of VAN proposed in the work of Zhong-Yu et al. (2018) [47], under typical conditions, involves an initial hydrogenation step, to produce 4-

(hydroxymethyl)-2-methoxyphenol, also known as vanillyl alcohol (VAL), followed by hydrodeoxygenation to produce 2-methoxy-4-methylphenol, or creosol (CRE) (Figure 11).

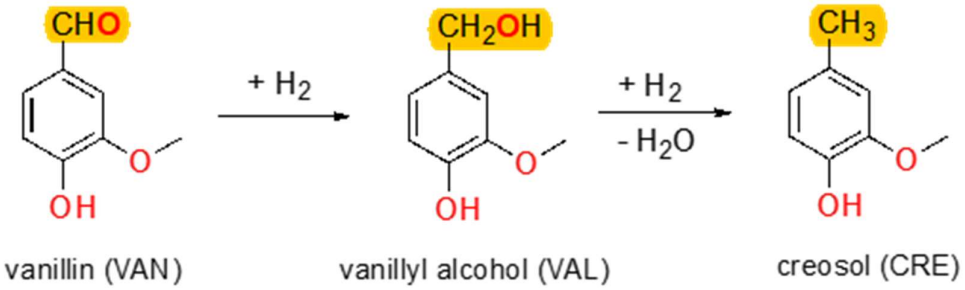

Figure 11. Reaction pathway in HDO of vanillin.

4.3 Palladium's role

As a significant phenolic compound, vanilline's multiple oxygen functionalities introduce specific challenges to HDO. To address this, catalysts that can efficiently cleave carbon-oxygen (C-O) bonds and drive the removal of oxygen atoms are highly sought after. Palladium (Pd) is a well-established catalyst in HDO reactions and has demonstrated proficiency in promoting hydrogenation and deoxygenation processes. A resume of works based on palladium catalyst applied in vanillin HDO is exposed in table 4.

Table 4. Reaction outcomes of HDO of Vanillin using Pd as active phase.

Sample	Reaction conditions	X (%)	S (%) CRE	Ref
Pd/C	110 °C,10 bar H_2, water, 2 h	> 99.5	79	[48]
Pd/MMF	110 °C, 10 bar H_2, water, 2h	> 99.5	71	[48]
Pd/TiO_2	110 °C, 10 bar H_2, water 2 h	> 99.5	17	[48]
Pd/γ- Al_2O_3	110 °C, 10 bar H_2, water, 2h	> 99.5	67	[48]
Pd/MSMF	110 °C, 10 bar H_2, water, 2h	> 99.5	> 99.5	[48]
Pd/C	100 °C, 10 bar H_2, octane-water, 3h	> 99	94	[49]
Pd-carbon Nitride	70 °C, 10 bar H_2, water, 1h	99	99	[50]
Pd/C	100 °C, 30 bar H_2, water, 3h	100	95	[51]
Pd/Norit	50 ◦C, 5 bar H_2, isopropanol, 5h	100	>99.5	[52]

One of the most valuable attributes of palladium, as highlighted in the literature and the recently introduced table, is its ability to facilitate HDO under milder reaction conditions compared to other catalytic systems. This aspect is particularly significant from a green chemistry perspective: milder reaction conditions imply a substantially lower use of energy and resources, a crucial feature for potential large-scale applications in the future. While the high cost of palladium might be a barrier for widespread use, its exceptional performance under less severe reaction conditions could offset this drawback.

4.4 Scientific approach

Acknowledging the well-established effectiveness of palladium, particularly its nanoparticles when supported, in facilitating hydrogenation reactions, palladium was selected as the focal metal. This choice was predicated on harnessing its renowned catalytic attributes. The quest for an efficient bimetallic catalyst in the hydrodeoxygenation (HDO) reaction of vanillin was methodically structured into three phases:

1. Selection of the best support for active phase;
2. Determination of the optimal Pd-Me (palladium-metal) bimetallic system;
3. Optimization of the Pd-Me ratio.

4.4.1 Support selection

The initiation of the catalytic optimization for the HDO reaction of vanillin commenced with an exhaustive investigation aimed at identifying the most effective support material. This inquiry systematically included a diverse array of supports, enabling a comprehensive evaluation. This strategic approach was intended to identify which support material could most effectively synergize with palladium, thereby enhancing the catalytic efficiency in the HDO process of vanillin. The objective was to optimize reaction conditions to achieve maximal catalytic performance, contributing to the advancement of sustainable chemical processes. The catalysts prepared and evaluated were:

- Pd/TiO_2,

- Pd/Nb_2O_5,

- Pd/SiO_2,

- Pd/AC (Activated Carbon).

Among these catalysts, palladium on titanium oxide and activated carbon have been unequivocally the most documented in literature and tested in reactions analogous or identical to the one described herein. For instance, in the study leaded by Souza et al. (2017) [53] examined various palladium-based catalysts on different supports, including TiO_2, aiming at the HDO reaction of various substrates. Specifically, for Pd/TiO_2 tested on phenol as a substrate, a conversion rate of 7% and a selectivity towards benzene of 66% were achieved within just 5 minutes of reaction time. The formation of benzene from phenol indicates a successful HDO reaction on phenol, suggesting that TiO_2 can enhance the catalytic activity of palladium's active sites.

Another significant study explored the active sites of palladium catalysts supported on carbon-based materials, tested in the hydrogenation and hydrodeoxygenation of benzaldehyde under very mild conditions (50 °C and 2 atm of H_2). This resulted in a 12% selectivity to toluene, a product derived from HDO reaction step, at best, with a 40% conversion of the reactant [54]

4.4.2 Bimetallic System Selection

After conducting experiments to ascertain which support yielded the best results, and thus would be utilized for subsequent catalysts, the focus shifted to selecting a metal to pair with palladium. This was achieved by testing the following bimetallic catalysts:

- $Pd\text{-}Pt/TiO_2$,

- $Pd\text{-}Sn/TiO_2$,

- $Pd\text{-}Au/TiO_2$,

- $Pd\text{-}Ag/TiO_2$.

As already said in chapter Literature on bimetallic catalysts includes various studies demonstrating the efficacy of certain bimetallic catalytic systems. For example, [30] detailed a study on a palladium-zinc bimetallic catalyst supported on activated carbon

used on various lignin-representative substrates, including vanillin. The reaction with vanillin was conducted in methanol at approximately 14 atm of H_2 and a temperature of 150 °C. After 8 hours of reaction, >99% conversion and 81% yield of Creosol were achieved.

4.4.3 Optimization of Pd-Me Ratio

Following the selection of the metal to pair with palladium, tests were conducted to prepare new bimetallic catalysts supported on TiO_2 using the same methodology, with particular attention to the accurate weighing of precursors when the target ratio was significantly imbalanced. A minor variation could significantly alter the final ratio of the two metals, impacting the catalytic efficiency and selectivity of the reaction.

4.5 Sol-immobilization method

For the synthesis of the catalysts, the sol-immobilization method was employed. This method is predicated on the immobilization of metallic nanoparticles on solid supports through the synthesis of colloidal solutions, or "sols". The technique is particularly esteemed for its capacity to control the particle size, distribution, and morphology of the metal nanoparticles, thereby directly influencing the catalytic activity, selectivity, and stability of the catalyst. Typically, the preparation of a catalyst via the sol-immobilization method encompasses the following steps:

1- **Preparation of the Sol**: The process begins with the synthesis of a sol, which is a colloidal dispersion of metallic nanoparticles in a liquid medium, typically distilled water. Generally, as in the case of this study, the formation of the colloidal dispersion of nanoparticles occurs through the reduction of metallic salts in the presence of reducing and stabilizing agents to prevent the aggregation of the nanoparticles.

2- **Immobilization on Supports**: The colloidal nanoparticles are then immobilized on solid supports, such as carbon, metal oxides, or polymers, through various mechanisms of interaction, including physical, chemical, or electrostatic bonds. This step is crucial for the dispersion of the nanoparticles and for their stability on the support.

3- **Thermal Treatment and Activation**: After immobilization, the catalysts can be

subjected to thermal treatments to remove solvents or protective agents and to activate the catalytic surface. These treatments affect the final structure and catalytic properties of the material.

This methodology is underscored by its ability to finely tune the catalytic properties through precise control over the nanoparticle characteristics, which is essential for optimizing the catalyst's performance in specific reactions.

5 EXPERIMENTAL PART

5.1 Catalysts synthesis

In the following subsections, the steps of the procedure are outlined in accordance with the synthesis technique described earlier.

5.1.1 Preparation of the Sol

To achieve a colloidal dispersion of metallic nanoparticles, a solution containing the metal precursors for the desired final catalyst was prepared (Figure 12). The precursors (Table 5) were added to achieve a final metal concentration in the solution of 0.13 mmol L^{-1}. This solution was maintained under stirring at room temperature throughout the synthesis process. For the actual formation of nanoparticles, a reducing agent was subsequently added, facilitating the reduction of metals in the precursors to their zero-oxidation state (0), thus enabling the formation of nanoparticles.

Table 5. Metal precursors used for nanoparticles suspension formation.

Nanoparticle's metal	**Metal precursor**
Pt	H_2PtCl_6, 8wt% solution, Sigma-Aldrich
Pd	K_2PdCl_4, 99.99%, Sigma-Aldrich
Sn	$SnCl_2$, 99.99%, Sigma Aldrich
Ag	$AgNO_3$, 99.99%, Sigma Aldrich
Au	$HAuCl_4 \cdot 3H_2O$, 99.99%, Sigma Aldrich

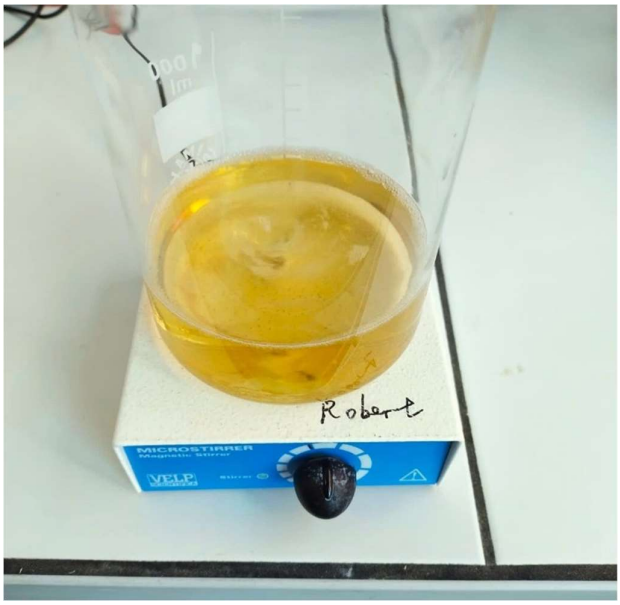

Figure 12. Preparation of the sol.

5.1.2 Immobilization of Metallic Nanoparticles

Polyvinyl alcohol (PVA) was used as the stabilizing agent. PVA is a commercially available polymer that is water-soluble, biocompatible, possesses low toxicity, and is slowly biodegradable. Furthermore, it has been documented to exert a stabilizing effect on colloidal solutions prepared in aqueous media [55], making it a widely studied and employed stabilizing agent over time. Following the preparation of the sol, a PVA solution was prepared by dissolving 0.0505g of PVA in 5mL of distilled water. This was then added to the metallic nanoparticle solution to achieve a final PVA/metal weight ratio of 1.2:1. Three minutes after the addition of PVA, a fresh aqueous solution of the reducing agent sodium borohydride ($NaBH_4$) was introduced to achieve a $NaBH_4$:metal molar ratio of 5:1. The reduction process typically results in an immediate change in the solution's colour due to the reduction of the metals and to the plasmon resonance phenomenon of nanoparticles [56]. Specifically, for Pd and Pt, a transition to various shades of grey is observed, indicating the successful formation of metal nanoparticles (Figure 13).

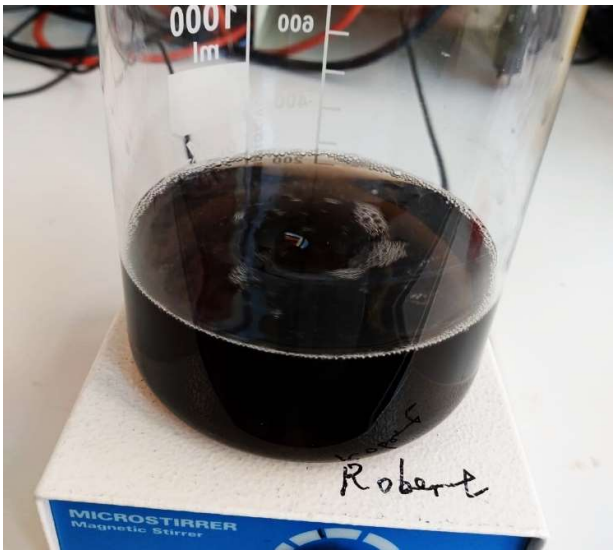

Figure 13. PVA and reductive agent addition step.

After an additional 30 minutes, support powder was added, and the solution was acidified, adjusting the pH with concentrated H_2SO_4 to below the isoelectric point of the specific support, to maximize interactions between it and the nanoparticles (table 6). Subsequently, the solution was stirred for another hour (Figure 14) before being allowed to settle, facilitating the sedimentation of the formed catalyst particles (Figure 15), which were then easily filtered using a Büchner filter (Figure 16).

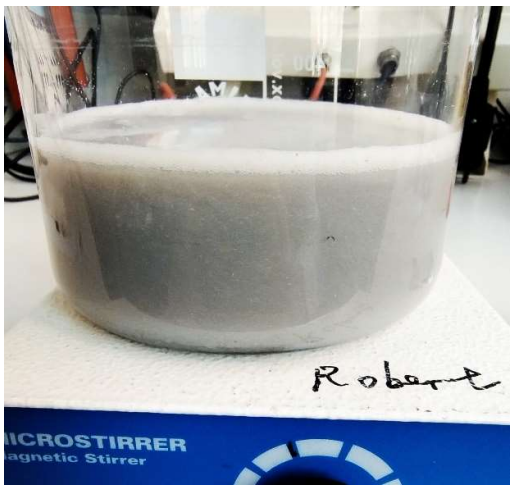

Figure 14. Support addition and acidification step.

Figure 15. Catalyst sedimentation.

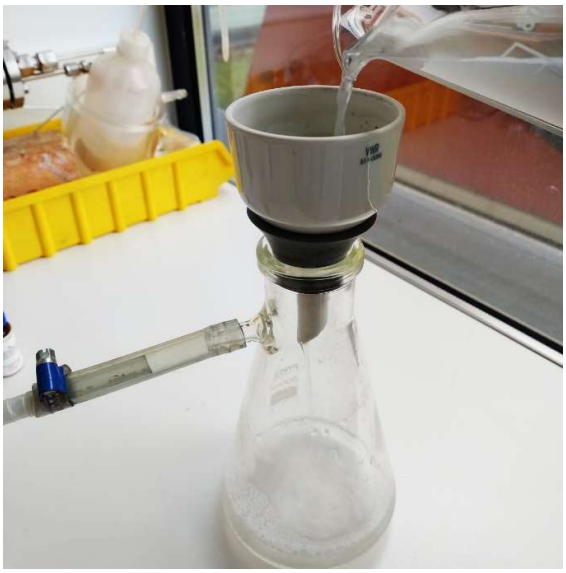

Figure 16. Filtration step.

Table 6. product used for the implementation of the support in catalysts synthesis and the corresponding target pH in H_2S0_4 addition step.

Support	Product used	Target pH
TiO_2	TiO_2 P25, 99.5%, Sigma-Aldrich	5
Activated carbon	Activated carbon	2
Nb_2O_5	Nb_2O_5 99.5%, Sigma-Aldrich	5
SiO_2	SiO_2 mesoporous SBA-15, Sigma Aldrich	4

5.1.3 Pre-Use Treatments

The catalyst was then washed with abundant distilled water (approximately 1 L) to remove impurities, until the wash water reached a neutral pH (Figure17). It was left to dry overnight at room temperature and further dried in an oven for 4 hours at 80°C (Figure 18). After this, the catalyst was easily scratched from the surface of the filter, weighed and stored in a small glass vial.

Figure 17. Catalyst just filtered.

Figure 18. Catalyst after thermal treatment.

All catalysts, both mono- and bi-metallic, were synthesized to achieve a final weight of 1g with a total metal loading of 1 wt%. The method, barring procedural errors, consistently provided an excellent yield in terms of weight. A synthetic scheme of the synthesis path is shown in Figure 19.

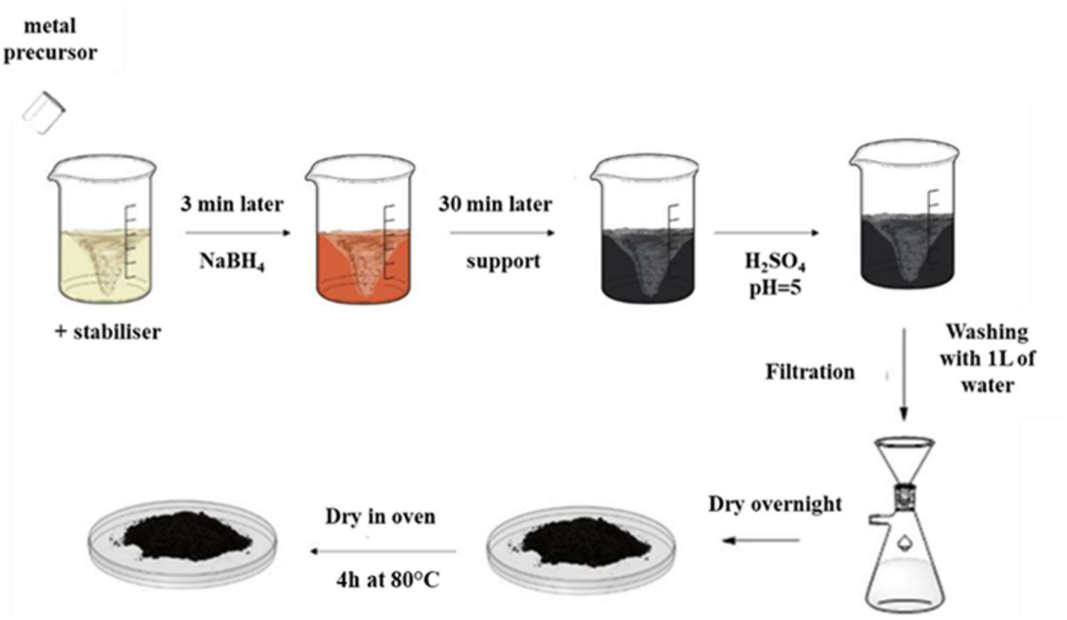

Figure 19. Scheme of the catalyst's synthesis path.

5.2 Catalytic Tests

Catalytic experiments were conducted within a 10 mL stainless steel batch bespoke reactor. The diminutive dimensions of the reactor facilitated adequate stirring and heating, achieved via a stir-hot plate equipped with a temperature control unit and a magnetic stirrer. The reactor is equipped with a custom thick copper plate, in which the reactor can be encased (Figure 20). The purpose of this copper plate is to make the heat transfer to the reactor and its contents as homogeneous as possible. The reactor is also equipped with three ports on top (Figure 21), to which have been connected:

a) hydrogen feed line, originating from a cylinder regulated by a pressure valve;
b) a thermocouple, interfaced with an inner temperature indicator;
c) a vent valve for the reactor.

Figure 20. Reactor placed in its apposite copper plate.

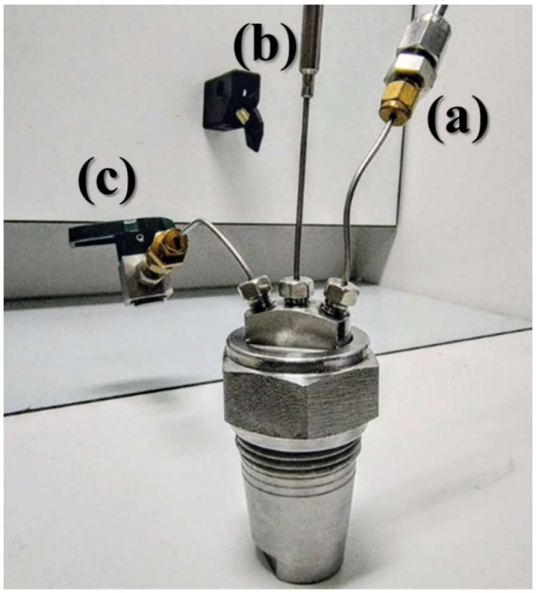

Figure 21. Reactor equipped with: a) hydrogen feed line; b) thermocouple and c) vent valve.

The temperature controller, connected to the heating plate, was linked to the system by creating a small hole in the copper plate, due to the impossibility of directly connecting the controller inside the reactor. Despite the temperature controller not being directly

connected inside the reactor, no issues were noted in maintaining the correct reaction temperature.

After the installation of the thermocouple, the vent valve and the H_2 feed line, with all the connections and reduction needed, leaks were tested with a leak detection solution. All the system was put under hydrogen pressure and the solution is applied in all the connections: if any leaks occurred, bubbles could be visible and leak from the connections detectable.

5.3 Choice of the solvent

To perform a reaction in liquid phase, one of the most important first things to consider is the choice of the solvent. HDO reactions are typically under H_2 pressure, but some very rare cases, thus, the property of the solvent to absorb the H_2 from reaction ambient becoming crucial for the outcomes, in the study carried by Aliu et al. (2021) [57] Diverse solvents were tried and, at same reaction conditions, various outcomes were reached (Table 7):

Table 7. Reaction performances obtained using different solvents [37].

solvent	X% VAN	S% VAL	S% CRE
Water	77	59	41
ehtylacetate	99	7	93
2-propanol	100	0	100
tetrahydrofuran	90	4	96
toluene	95	47	53
cyclohexane	70	97	3

These results indicates that vanillin easily hydrogenates under the various solvents, and it has been noted that the highest activity achieved in polar protic solvents and the lowest activity in aprotic polar solvents. H_2 uptake was analysed, and every solvent showed a different behaviour through reaction time (Figure 22 [57]).

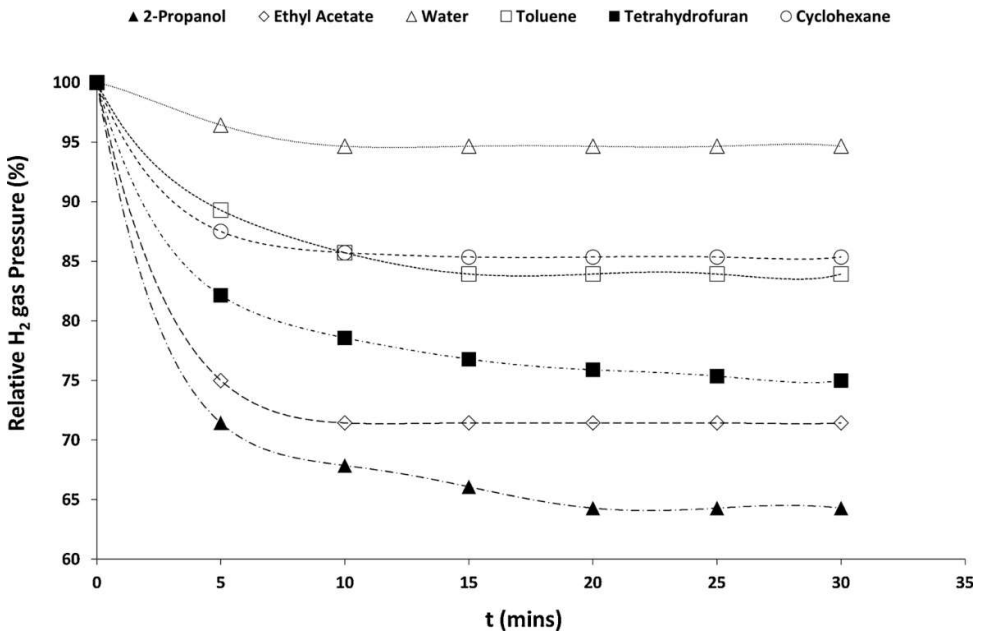

Figure 22. H_2 uptake of different solvents during reaction time.

Turnover frequency (TOF, a rate metric indicating the number of reactant molecules converted by a single catalytic site per unit time) of every reaction was calculated and, notably the trend in TOF values follows the same pattern observed from H_2 uptake. In the work, it has been noted that the adsorption of a polar reactant such as vanillin should be more favourable in non-polar solvents such as toluene and cyclohexane [58], but reduced catalytic activity was observed in these solvents because of the low H_2 uptake, indicating the importance of this parameter.

The performances carried out from the use of isopropanol guided the choice of isopropanol as a solvent for reactions executed in this work.

5.4 Reaction Run

Initially, 100 mL of a vanillin solution in isopropanol with a concentration of 10 g/L was prepared, dissolving the solute effortlessly. The reactor was weighed before and after adding each reaction component to monitor the actual amounts of substrate and catalyst. Given the solvent's high volatility, the reactor's weight was also checked at the start and end of the reaction to quantify any solvent loss while the reactor was open for sample collection. This consideration allowed for adjusting the real concentrations in each reaction mix's final composition. For a typical test, 0.015g of catalyst and 5 mL of the vanillin solution were introduced to achieve a VAN/metal molar ratio of about 400.

The reactor was then sealed and purged with hydrogen gas under typical conditions of 3 bar of H_2, 20 °C, and stirring at 300 rpm.

In some experiments the temperature and pressure were changed to 80 °C and 8 bar, respectively. Reaction time was typically 30 mins but there were tests also at shorter (minimum 15 minutes) and longer (maximum 4h) time. After the reaction time, the stirring was stopped, and pressure was gradually released with the vent valve. In cases of high temperature tests, the heating has also been stopped and, before opening the vent valve, room temperature was reached. The reaction mixture was then filtered through a PTFE syringe filter directly into a 2 mL vials for subsequent GC-MS analysis.

5.5 Qualitative and Quantitative Analysis via Gas Chromatography

Gas chromatography (GC) stands as a pivotal technique in the realm of chromatography, focusing on the separation of compound mixtures into distinct entities. This separation facilitates both the qualitative identification and quantitative measurement of the mixture's components. Among the assortment of chromatographic methods and their respective instruments, GC is noteworthy. It is approximated that GC can analyze 10-20% of known compounds, contingent upon their volatility and thermal stability. For a compound to be deemed appropriate for GC, it must exhibit sufficient volatility and remain stable without decomposing at temperatures up to 400-450 °C.

In GC, one or several high-purity gases are utilized, with one designated as the carrier gas. This gas propels through the injector, traverses the column, and finally reaches the detector. Samples are introduced into the injector, typically via a syringe or an external sampling mechanism, where they are heated to 150-250 °C. This heating process vaporizes the volatile solutes, which are then transported through the column by the carrier gas. The column itself is situated within a temperature-regulated oven, ensuring that solutes progress at rates influenced by their physical properties, as well as the column's temperature and composition. As solutes elute at varying rates, each is detected upon exiting the column, with their interaction with the detector generating an electronic signal. This signal is recorded and visualized as a chromatogram, plotting signal magnitude against time elapsed.

An optimal chromatogram features peaks that are well-defined and non-overlapping. Key metrics such as retention time and peak intensity serve critical roles in identifying and quantifying compounds within the sample. The peak's area directly correlates with the compound's concentration in the sample, with larger peaks indicating higher concentrations. Maintaining constant column and operational conditions ensures consistent retention times for compounds, facilitating their identification through comparison with known commercial standards.

However, challenges arise when peaks overlap or share identical retention times, complicating accurate measurement and identification. Hence, achieving distinct peaks without co-elution is essential for precise analysis.

5.5.1 Qualification by Mass spectroscopy

Gas Chromatography-Mass Spectrometry (GC/MS) is a sophisticated analytical method that integrates gas chromatography (GC) with mass spectrometry (MS) to separate, detect, and quantify complex mixtures of chemical substances. This technique is particularly effective for analysing a wide array of low molecular weight compounds present in environmental samples. For successful GC/MS analysis, the compounds under investigation must be volatile and stable under high temperatures. Moreover, compounds with functional groups may undergo derivatization to prevent unwanted adsorption phenomena, enhancing the accuracy of the analysis. Typically, samples such as soils, sediments, and biological tissues are extracted with solvents, and these extracts are then treated with various chemical processes prior to GC/MS analysis.

Upon injection into the GC system, the sample is vaporized in the inlet and carried through a chromatographic column by a carrier gas, commonly helium. As the sample progresses through the column, its constituent compounds are separated based on their interactions with the column's stationary phase and the mobile phase carrier gas. Exiting the column, the compounds enter an ion source via a heated transfer line, where they are ionized before mass spectrometric analysis.

Ionization in GC/MS can be achieved through two primary methods: electron ionization (EI) and chemical ionization (CI). EI involves bombarding the sample molecules with electrons, leading to the formation of molecular ions (M^+), which are radical cations.

This process often results in the fragmentation of the molecular ion, creating a pattern of smaller ions unique to the molecular structure of the compound. This "fingerprint" aids in identifying specific compounds and elucidating the structures of unknown molecules within a mixture. Alternatively, CI ionizes the sample molecules by interaction with ionized methane or another gas, producing $[M+H]^+$ ions. This method is gentler, causing less fragmentation and providing the molecular weight of the compound, though it offers less structural detail than EI. Both ionization techniques are complementary, offering a comprehensive view of the molecular ions and their fragments.

Following ionization, ions are propelled into a mass analyser, which sorts them based on mass-to-charge ratios. Various analysers are employed, including quadrupoles and ion traps, which are among the most prevalent. The ions are then detected, and the resulting signals are amplified and transmitted to a computer. This computer not only visualizes the data but also oversees the mass spectrometer's operations, ensuring precise control over the analytical process. Through GC/MS, researchers can obtain detailed information about the chemical composition of complex mixtures, making it an indispensable tool in environmental chemistry and beyond.

5.5.1.1 Reaction products' retention times and MS spectra

Vanillin: Retention time ≈ 19.2 min

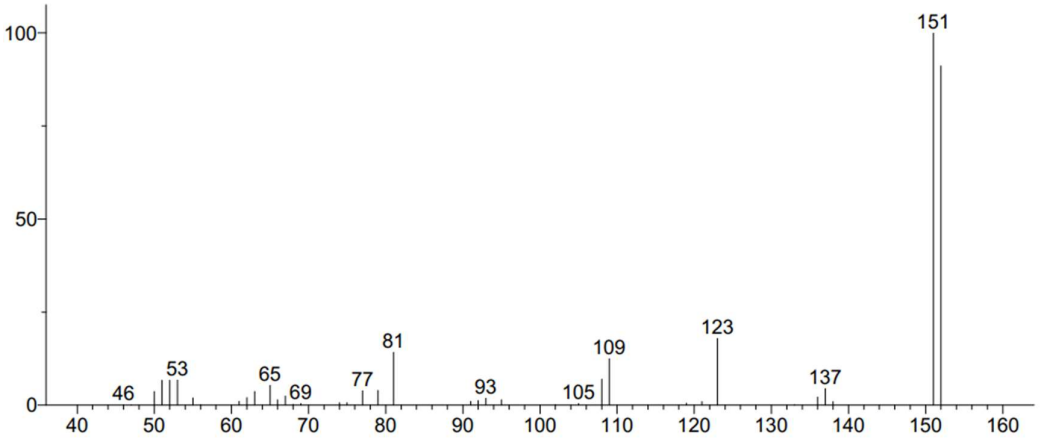

Vanillyl alcohol: Retention time ≈ 19.9 min

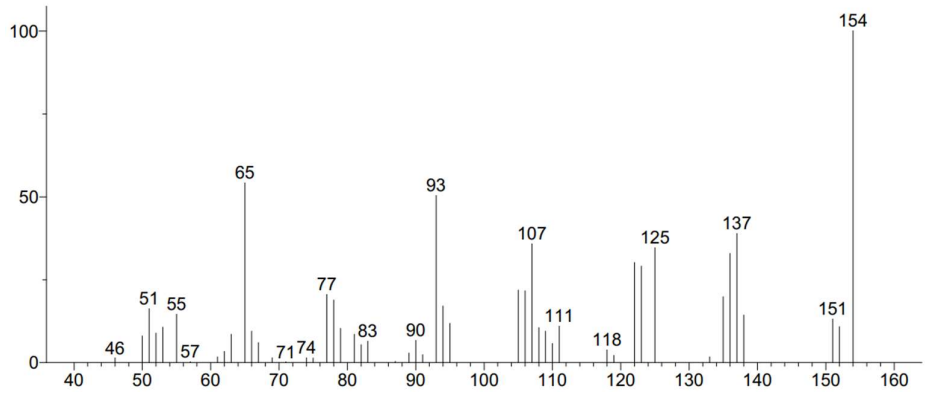

Creosol: Retention time ≈ 15.3 min

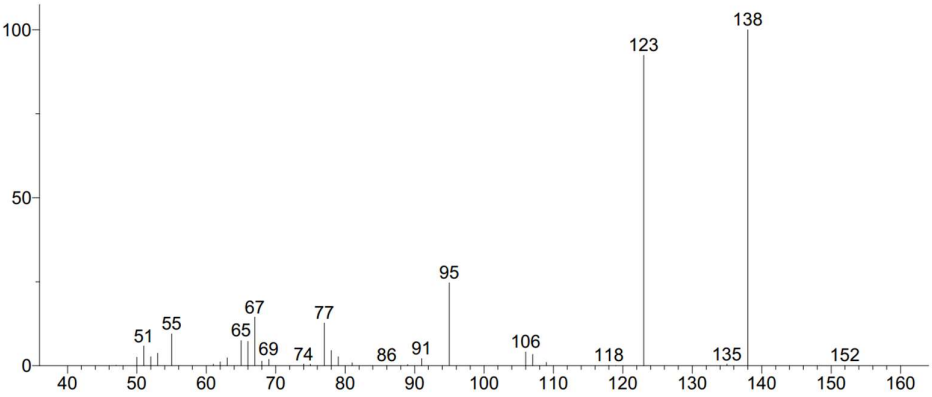

5.5.2 Quantification by Flame Ionization Detection

The Flame Ionization Detector (FID) is a highly sensitive method used for detecting and quantifying organic compounds in gas chromatography. This process ionizes carbon atoms, producing ions and electrons that generate a measurable electrical current proportional to the carbon content, enabling precise quantification.

FID stands out for its wide linear response range, allowing for accurate measurement of compounds at both trace and high concentrations. Its sensitivity to hydrocarbons and insensitivity to inorganic gases or water vapor make it suitable for environmental and petrochemical analyses.

The instrument used is a gas chromatograph coupled with a mass spectrometer and flame ionization detector (GC-MS/FID, Agilent Technologies 5977B MSD), employing a CP-wax 52 CB column (polyethylene glycol phase, 30 m x 250 μm, 0.250 μm), capable to qualify and quantify the sample simultaneously. The conditions of the GC analysis are shown in Table 8:

Table 8. List of GC analysis conditions.

Injection	Injection mode	Split-Splitless Inlet
	Temperature	250 °C
	Carrier gas	He
	Pressure	13.6 psi
	Total flow	24.69 mL min^{-1}
	Column flow	mL min^{-1}
Oven	Initial temperature	40°C (3.5 min)
	T1	150°C (15 °C min^{-1}) / 1 min
	T2	195 °C (25°C min^{-1}) / 2 min
	T3	205 °C (2°C min^{-1}) / 1 min
	T4	150 °C (20°C min^{-1}) / 10 min
	Equilibration time	0.25 min
	Total program time	33.88 min
	Final temperature, Tf	250 °C
Detector (FID)	Temperature	270 °C
	H_2 flow	40 mL min^{-1}
	Air flow	400 mL min^{-1}

5.5.3 Calibration of GC

Product quantification for each reaction was conducted by establishing calibration curves for every product, utilizing a series of dilutions from a master mix of reaction components VAN, VAL, CRE, each at a concentration of 10 g/L. This process resulted in the preparation of standards at six different concentrations: 10, 8, 6, 4, 2, and 1 g/L. GC-MS/FID will give a signal in form of an area for each compound, with calibration curves built it is possible then associate that area to a specific concentration. Below are reported the three calibration curves obtained:

- Vanillin calibration:

Peak area	Conc (g/L)
20508775.34	10.93
16986055.83	8.744
12282184.38	6.558
8175216	4.372
4013764.37	2.186
1874499.71	1.093

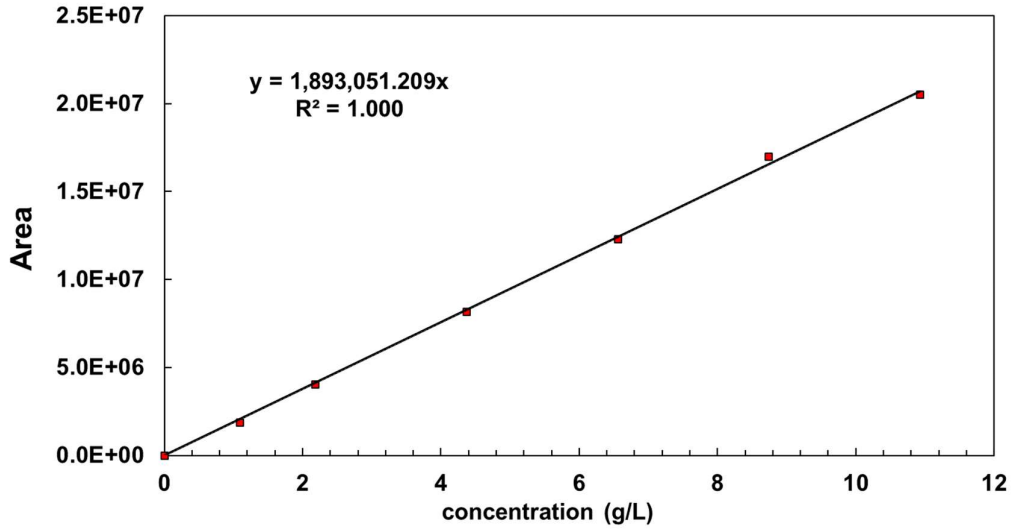

- Vanillyl Alcohol calibration:

Peak area	Conc (g/L)
16574166.4	10.4566
14080106.12	8.36528
10301524.02	6.27396
6520571.91	4.18264
2566959.18	2.09132
1021716.29	1.04566

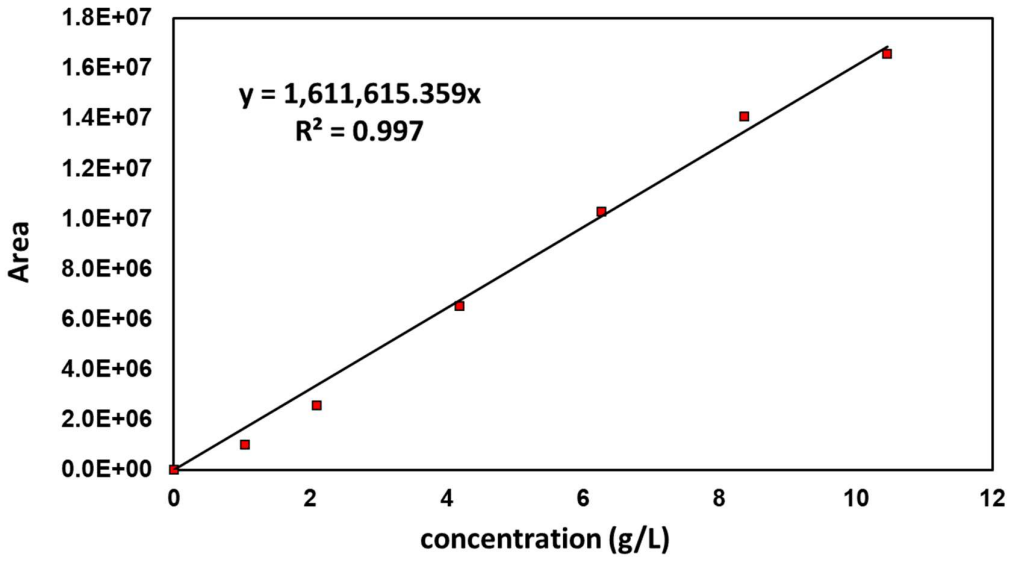

-

- Creosol Calibration:

Peak area	Conc (g/L)
24785824.63	10.52
19910585.71	8.416
14583056.53	6.312
9453432.52	4.208
4481327.07	2.104
2065305.85	1.052

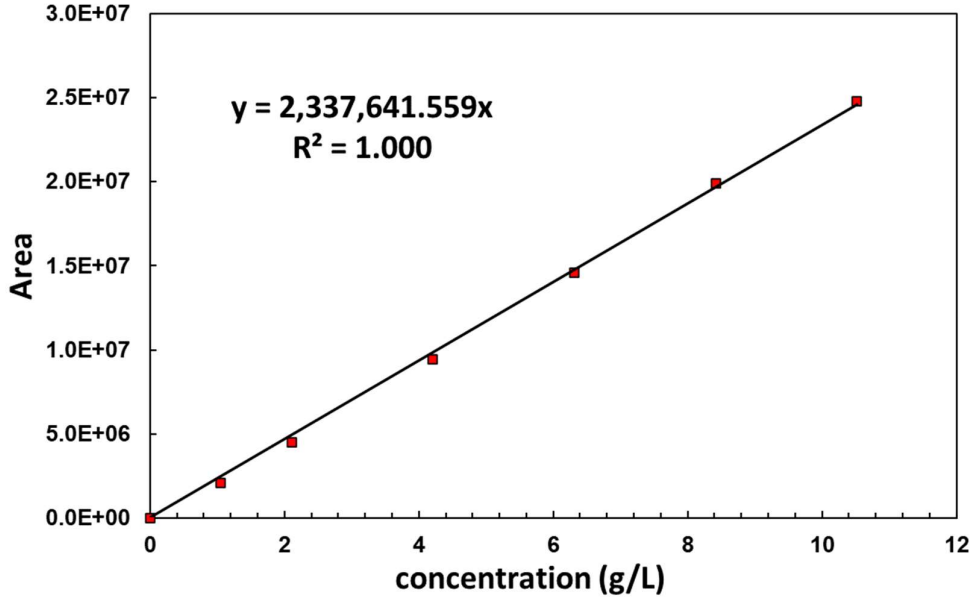

Through calibration, the exact concentration of products at the end of each reaction was calculated, allowing for the derivation of reaction performance metrics. The conversion rate (X%) was calculated using the equation:

$$Conversion\ = \frac{mol_i\ - mol_f}{mol_i} \cdot 100$$

Where mol_i represents the initial moles of VAN, and mol_f are the moles at the end of reaction. Selectivity (S%) was determined as follows:

$$Selectivity_a = \frac{mol_a}{\sum\ mol_n} \cdot 100$$

Where mol(a) are the moles of product at the end of the reaction, and $\sum\ mol_n$ are the sum of moles of all the products at the end of reaction. Catalytic activity (A) was calculated using the equation:

$$Reaction\ Rate\ (h^{-1}) = \frac{mol_i - mol_f}{mol_m \cdot t}$$

Where mol (m) is the sum of the moles of metal present in the reaction, and t is the time of reaction, expressed in hours.

5.6 Catalyst characterization

5.6.1 Inductively Coupled Plasma Optical Emission Spectrometry (ICP-OES)

ICP-OES is a powerful analytical technique widely used for the characterization of heterogeneous catalysts, particularly in determining metal loading. This capability is crucial for understanding the catalytic performance, as the amount and distribution of active metal sites directly influence the activity, selectivity, and stability of catalysts. ICP-OES operates on the principle of exciting atoms in a sample to emit light at wavelengths characteristic of specific elements. By measuring the intensity of this light, the concentration of elements within the sample can be quantified. This technique is especially beneficial for characterizing metal loadings in heterogeneous catalysts due to its:

- High Sensitivity and Accuracy: Capable of detecting trace levels of metals, essential for catalysts where active components are often present in low concentrations.
- Wide Dynamic Range: Allows for the quantification of both major and minor components within the same analysis.
- Multi-element Capability: Enables simultaneous detection of multiple metal species, useful for complex catalyst systems containing several active metals.
- Minimal Interference: The capability to resolve spectral interferences enhances the accuracy of metal quantification.

In the case of this work, ICP-OES analysis was performed using Agilent 720-ES ICP-OES equipment combined with Vulcan 42S automated digestion system.

5.6.2 X-ray diffraction (XRD)

XRD is a powerful analytical technique that utilizes the diffraction of X-rays by the crystalline structures within materials to be able to understand their structural properties. The principle of XRD analysis involves the interaction of X-ray beams with the electron clouds of atoms within a crystalline lattice, resulting in a diffraction pattern that is characteristic of the material's internal structure. By analysing these diffraction patterns, it is possible identify the crystallographic phases present, quantify phase abundances, and discern structural modifications that occur during catalytic reactions. This information is essential in the design and optimization of catalysts, as it aids in correlating the structural attributes of the material with its catalytic performance.

5.6.3 Transmission electron microscopy (TEM)

TEM operates by transmitting a beam of electrons through a very thin sample. The electrons interact with the sample as they pass through it, producing an image or a diffraction pattern that can be observed on a screen or detector. This technique allows for the direct visualization of the catalyst's morphology at the nanometer or even atomic scale. TEM can provide high-resolution images of catalyst particles, revealing their shape, size, and distribution on a support material. This is crucial for catalysts where the active component is dispersed as nanoparticles.

Transmission Electron Microscopy (TEM) images were recorded by placing a drop of the particle's dispersion in isopropanol over a carbon film supported on a copper grid. FEI Tecnai microscope was used for the recording of the images. More than 600 particles were used for the distribution size studies. It was performed using Image J software.

5.6.4 Scanning Transmission Electron Microscopy (STEM)

STEM is a variation of traditional TEM that combines the principles of both scanning electron microscopy (SEM) and TEM to offer detailed insights into the structure and composition of materials at the atomic scale. In STEM, an electron beam is focused into a fine probe and then systematically raster-scanned across the sample. As the beam interacts with the sample, various signals are generated, including secondary electrons, backscattered electrons, and transmitted electrons. These signals can be collected to form images or to conduct spectroscopic analysis. For the analysis of individual nanoparticles, STEM was performed on a TITAN Themis 300 S/TEM microscope equipped with:

- a probe aberration corrector and monochromator, allowing spatial resolution of 70 pm and energy resolution of 150 meV;
- a super-X windowless 4 quadrant SDD (silicon drift detector) detection system for STEM-EDX mapping and several annual dark field detectors;
- a high-resolution post column GIF, the GATAN's Quantum ERS/966 with 2kx2k Ultrascan camera with 994G sensor, for the acquisition of electron energy loss spectra.

5.6.5 High-angle annular dark field (HAADF)

In order to investigate the elemental distribution within bimetallic particles, high-angle annular dark field (HAADF) imaging and high-resolution electron energy loss spectroscopy (HR-EELS) were carried out in the STEM mode. Measurements were performed with a spot size of about 500 pm, a semi-convergence angle between 16 and 21 mrad, and a probe current of approximately 100 pA. For HAADF images, collection angles were chosen between 50 and 200 mrad. Dual EELS acquisition was performed

in the spectral imaging mode with a collection angle of 49 mrad, a dispersion of 0.25 eV/ch, a step between 150 and 700 pm, and a dwell time between 50 and 200 ms. Alignment of the energy drift was done on the zero-loss peak. When possible, noise reduction by PCA was performed on the spectrum images using HyperSpy.

5.6.6 X-ray Photoelectron Spectroscopy (XPS)

XPS is a surface-sensitive quantitative spectroscopic technique that measures the elemental composition, empirical formula, chemical state, and electronic state of the elements that exist within a material. XPS works by irradiating a material with a beam of X-rays, causing the emission of photoelectrons from the surface layers of the material. The kinetic energy and the number of electrons that escape from the top 1 to 10 nm of the material are measured. Because the kinetic energy of the electrons is characteristic of the elements from which they were emitted, this information can be used to identify the elements present on the surface of the sample. Additionally, the binding energy of the electrons provides information about the chemical state of the elements, allowing for the differentiation between different oxidation states or chemical environments.

The analysis was performed on an XPS Kratos, Axis UltraDLD “2009” with monochromatic Al Kα ($h\upsilon$=1486.6 eV) radiation as the excitation source and equipped with high-performance hemispheric analyzer. Calibration of the binding energies was performed using the carbon C 1s reference at 284.8 eV.

6 RESULTS AND DISCUSSION I – CATALITIC TESTS

6.1 Influence of the support

To elucidate and examine the optimal bimetallic catalytic system, a preliminary investigation was undertaken to compare different supports for Pd monometallic catalysts. Four different catalysts were prepared using the sol-immobilization method described in chapter 2, all based on palladium with four distinct supports. To summarize, the prepared catalysts were: Pd/TiO_2, Pd/Nb_2O_5, Pd/SiO_2, and Pd/AC.

Following the preparation of these catalysts, they were tested under identical reaction conditions: reaction time of 1 hour, 3 atm of hydrogen, 300 rpm of magnetic stirring, 5 mL of a vanillin solution with a concentration of 10 g/L, and 15 mg of catalyst. The outcomes of the reactions are presented in the Table 9 and Figures 23 and 24.

Table 9. Resume of catalytic performances of Pd catalysts obtained varying the support utilised.

Catalyst	X% Van	Y % CRE	Y% VAL	Activity
Pd/AC	100.00	34.34	65.66	251.36
Pd/TiO_2	99.36	32.03	66.05	292.47
Pd/SiO_2	40.03	0.00	40.03	94.73
Pd/Nb_2O_5	100.00	41.83	56.47	223.65

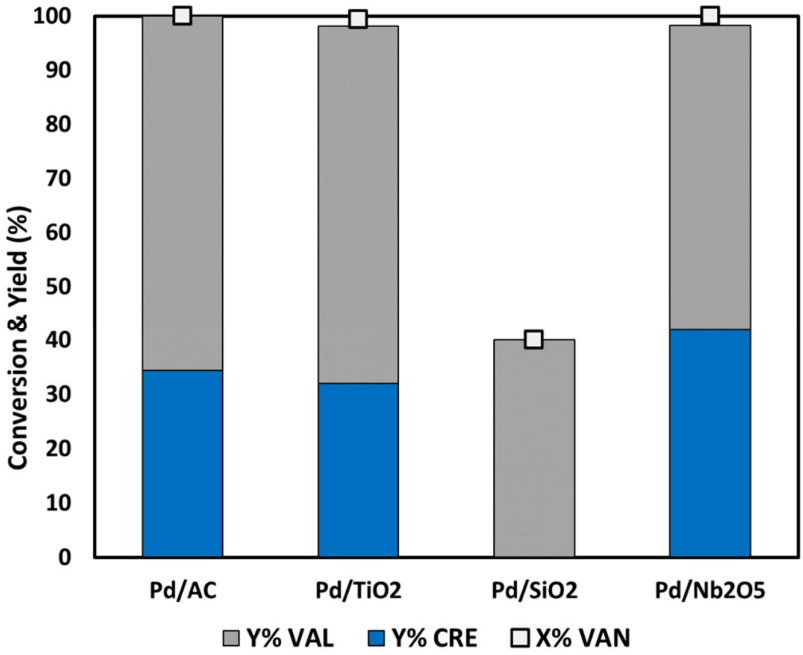

Figure 23. Catalytic performances of palladium catalysts varying the support utilised.

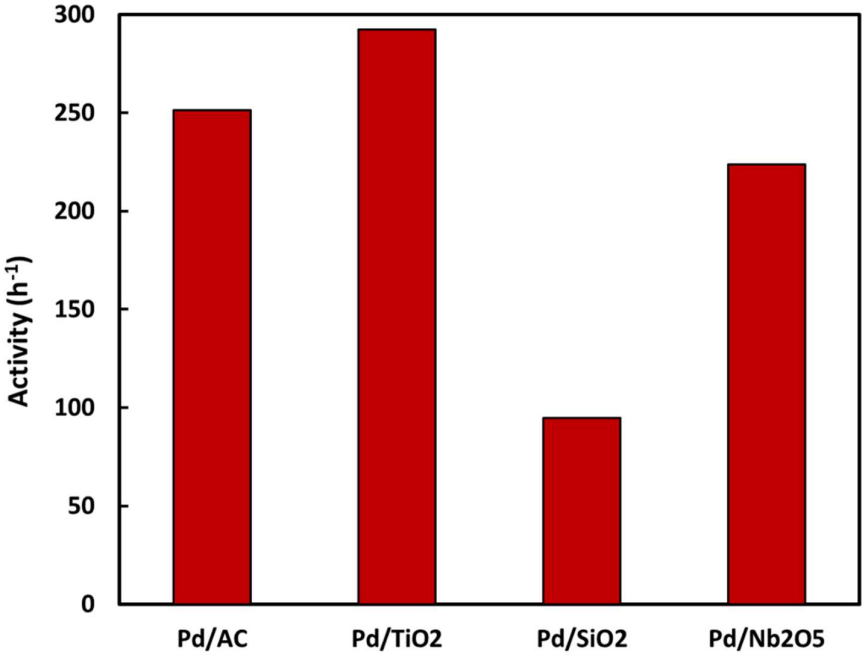

Figure 24. Catalytic activity of palladium catalysts varying the support utilised.

The results presented indicate that the choice of support material significantly impacts the catalyst's activity. Catalysts supported on TiO_2, AC and Nb_2O_5 showed good performances at 20°C, while the SiO_2-based catalyst exhibited no activity for the hydrodeoxygenation (HDO) step of the reaction pathway, with no presence of creosol detected under the tested conditions and the lowest reaction rate between the catalysts tested. The other catalysts demonstrated a markedly higher capability in converting vanillin, achieving a conversion rate of 100% or similar. Additionally, a creosol yield exceeding 30% was observed for all three tested catalysts, with Nb_2O_5 reaching up to 40%.

Between these three best supports, TiO_2 was chosen for further studies. The selection of TiO_2 for further studies despite the similar activity observed among Pd/TiO_2, Pd/Nb_2O_5, and Pd/AC catalysts is primarily driven by its favourable characteristics in comparison to the other two catalysts. Firstly, while all three catalysts exhibit similar activity, the slightly higher reaction rate observed for the TiO_2-based catalyst suggests that TiO_2 may offer improved performance under specific reaction conditions. Secondly, the decision to opt for TiO_2 over Nb_2O_5 is influenced by the desire to avoid the high acidity associated with Nb_2O_5, due to the presence of Lewis acid sites [59]. High acidity may increase the HDO reaction rate, however, it can also result in

unwanted side reactions, catalyst deactivation, and the formation of undesirable by-products. In fact, in the work made by Wang et al. (2020) [59], the focus is on the role of the catalyst support in HDO reactions, with a particular emphasis on the acid sites and the morphological characteristics of the support. It is noted that the presence of strong acid sites leads to high C-O bond dissociation rates. Specifically, using solid acid supports like HZSM-5, a type of zeolite, resulted in achieving 100% selectivity to cycloalkanes at full conversion of phenol. However, the document also points out that metal oxides containing Lewis's acid sites, such as silica and alumina, could overly strongly adsorb phenolic compounds. This, in turn, reduces the catalyst's activity. Additionally, it is reported that the gradual accumulation of substrates and intermediates containing oxygen can generate new active sites. These new sites could then steer the reaction towards the production of undesired products.

By choosing TiO_2, which typically exhibits lower acidity compared to Nb_2O_5, the risk of these issues is mitigated, ensuring better control over the reaction process and product selectivity. Moreover, the consideration of diffusion problems associated with the high surface area of activated carbon further supports the preference for TiO_2. Indeed, the extensive porous structure can sometimes lead to diffusion limitations, especially in complex reaction systems [60]. TiO_2, with its more structured and less porous nature, may alleviate these diffusion issues, resulting in more uniform and efficient catalytic performance. All these aspects are in agreement with the main objectives of this work, which concern the Pd-Me synergy studies.

6.2 Influence of the reaction conditions.

To elucidate the impact of reaction temperature and pressure on the catalytic process, a series of experiments were conducted varying these two parameters. Experiments were carried out changing temperature first: at 30 °C, 50 °C, and 80 °C, and secondly varying the hydrogen pressure from 1, 3, 5, to 8 atm, using Pd/TiO_2 as catalyst. Considering that the Pd/TiO_2 catalyst achieved a complete VAN conversion at 20 °C after only 1 hour, the duration of each reaction was set to 15 minutes. Before the initiation of each reaction, the system was purged with hydrogen three times. For each experiment, 5 mL of a vanillin solution with a concentration of 10 g/L and 15 mg of the catalyst were introduced. The reactions commenced with stirring, maintained at a constant speed of

300 rpm. The outcomes of the reactions are presented in the Tables 10 and 11 and Figures 25, 26, 27 and 28.

Table 10. Resume of catalytic performances of Pd/TiO_2 varying reaction temperature.

Temperature	X% VAN	Y% CRE	Y% VAL	Activity
20 °C	12.50	2.53	57.22	135.88
50 °C	100.00	25.40	66.67	1213.97
80 °C	99.45	44.54	47.25	1145.64

Reaction conditions. 3 atm H_2, 300 rpm, 5 mL of a 10 g/L VAN solution, 15 mg of catalyst, 15 min.

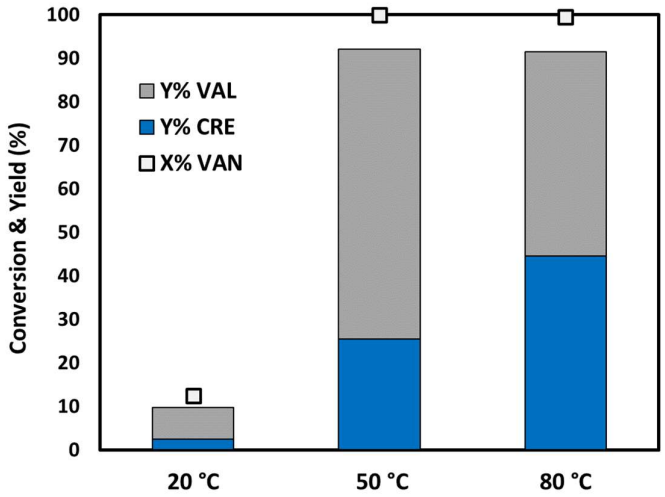

Figure 25. Catalytic performances of Pd/TiO_2 at different reaction temperatures.

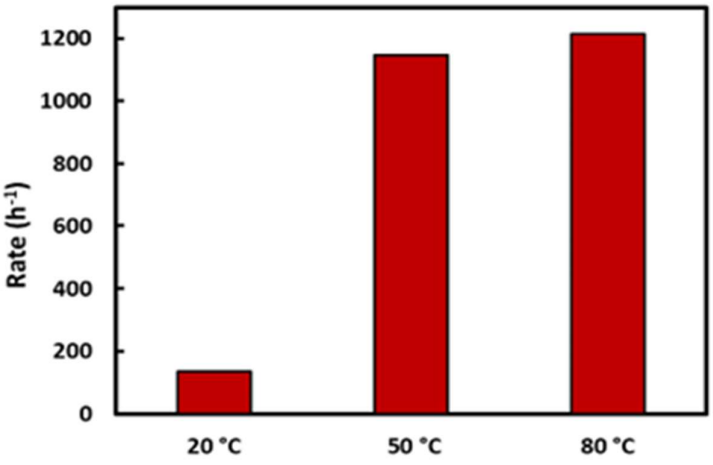

Figure 26. Pd/TiO_2 catalytic activity at different reaction temperatures.

Table 11. Resume of catalytic performances of Pd/TiO_2 at varying H_2 pressure.

Pressure (atm)	X% VAN	Y% CRE	Y% VAL	Activiy
1	4.60	0.00	4.60	49.28
3	12.50	2.53	7.15	135.88
5	16.45	3.30	13.15	159.19
8	15.89	3.38	12.51	152.58

Reaction conditions: 20°C, 300 rpm, 5 mL of a 10 g/L VAN solution, 15 mg of catalyst, 15 min.

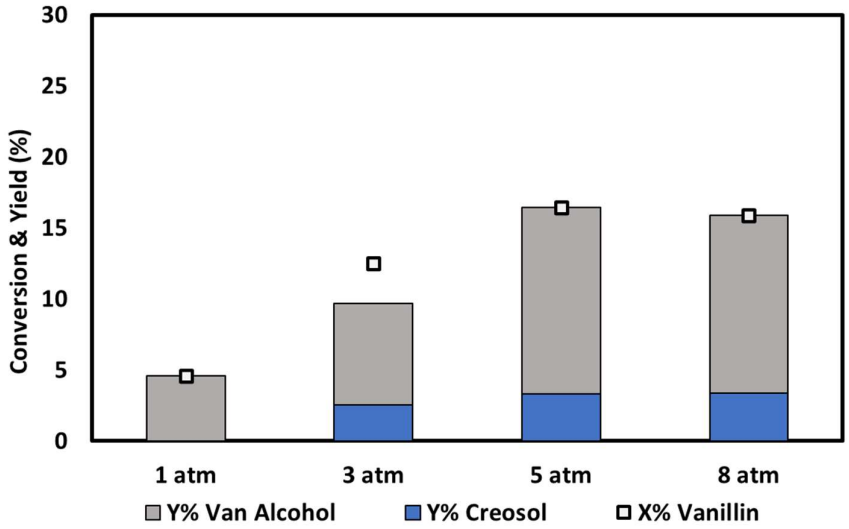

Figure 27. Catalytic performances using Pd/TiO_2 varying H_2 pressure.

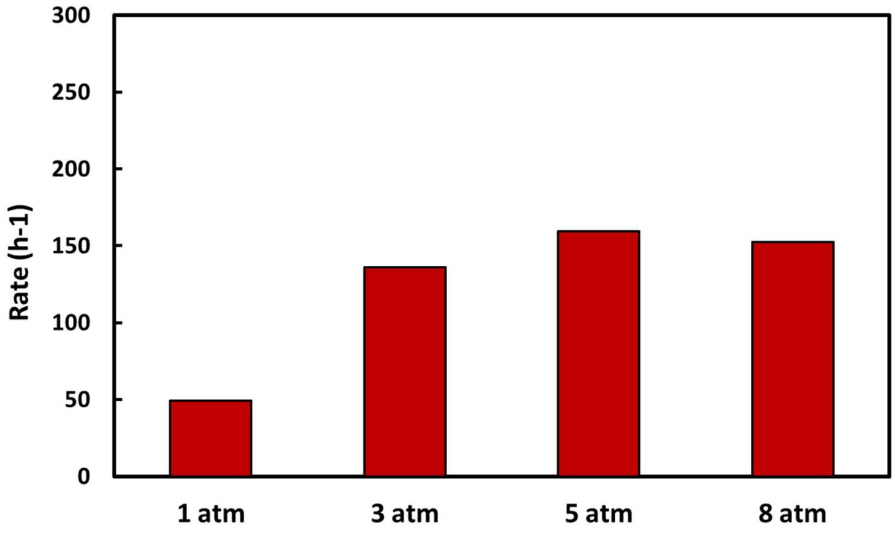

Figure 28. Catalytic activity of Pd/TiO_2 varying H_2 pressure.

Remarkable 100% of VAN conversion was observed after 15 min at 50 °C and 80 °C. An impressive catalyst rate of more than 1100 h^{-1} was reached at 50 °C and 80 °C, demonstrating an incredible reaction temperature sensitiveness. At 80 °C the CRE yield reached 45% after 15 min. The impact of pressure on the VAN conversion was observed to be moderate yet noteworthy. Specifically, VAN conversion increased from approximately 5% at 1 atm of hydrogen to nearly 20% when the pressure was elevated to 5 and 8 atm. This trend was consistent with the increases in catalytic activity under the same conditions. Conversely, the CRE yield remained largely unaffected by increments in H_2 pressure from 3 to 8 bars. These results suggest that, within the context of our experimental setup and reaction conditions, the optimal hydrogen pressure for desired reaction outcomes appears to have been achieved within this specified pressure range.

6.3 Influence of the second metal-loaded

Upon identifying the optimal support material for palladium nanoparticle catalysts, the synthesis of subsequent bimetallic catalysts supported on TiO_2 was undertaken using the sol-immobilization method. The prepared catalysts included PdPt/TiO_2, PdAu/TiO_2, PdSn/TiO_2, and PdAg/TiO_2. The target molar ratio between the two metals was maintained at 1:1 for each catalyst. Investigating the efficacy of these new bimetallic catalysts is crucial as it offers an initial assessment of which metals exhibit compatibility with palladium and could determine the presence of any synergistic interactions between the used metals. After the synthesis of the catalysts, they were employed in catalytic tests under identical reaction conditions: 1 hour, 3 atm of H_2, 300 rpm of magnetic stirring, 5 mL of vanillin solution at a concentration of 10 g/L, and 15 mg of catalyst. The outcomes of the reactions are presented in the table 12 and figures 29 and 30.

Table 12. Results of catalytic performances using Pd-Me/TiO_2 bimetallic catalysts.

Catalyst	X% VAN	Y% CRE	Y% VAL	Rate
PdAu/TiO_2	36.46	0.00	36.46	96.00
PdAg/TiO_2	23.24	1.63	21.61	57.45
PdPt/TiO_2	99.21	31.42	67.79	245.99
PdSn/TiO_2	8.41	0.00	8.41	34.18

Reaction conditions: 20°C, 3 bar H_2, 300 rpm, 5 mL of a 10 g/L VAN solution, 15 mg of catalyst, 1h.

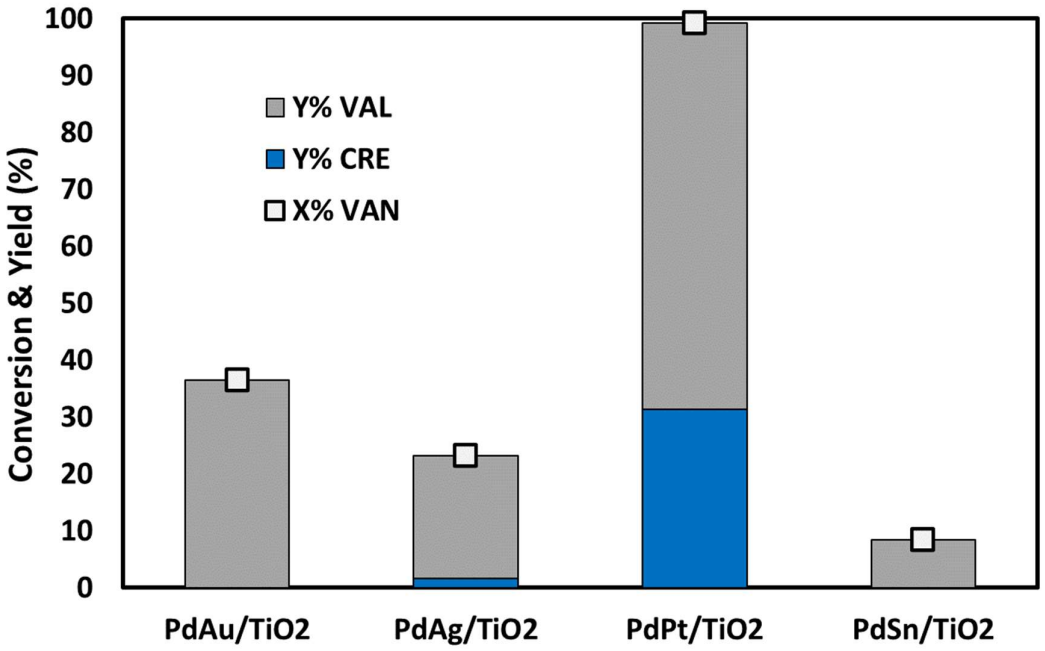

Figure 29. Catalytic performances of Pd-Me/TiO_2 bimetallic catalysts.

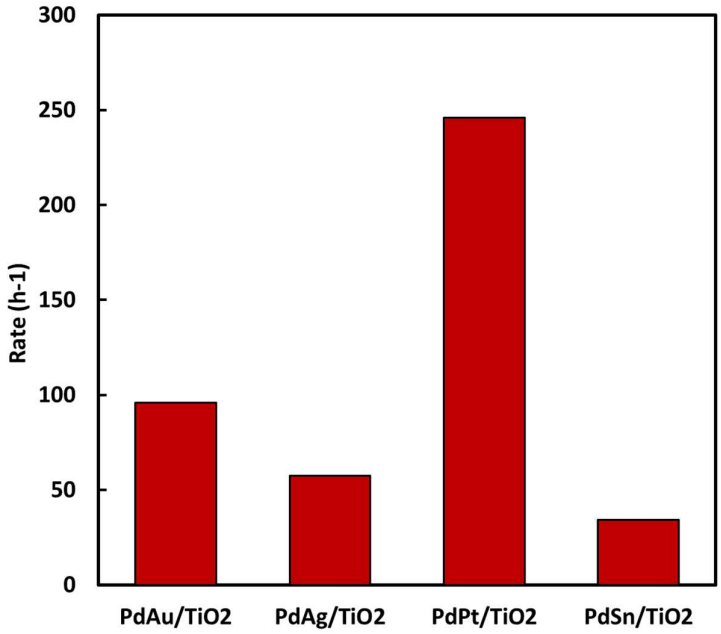

Figure 30. Catalytic activity of Pd-Me/TiO_2 bimetallic catalysts.

Pd-Au bimetallic catalyst showed no selectivity towards the desired product, creosol, with a conversion rate of 36.46% and 100% selectivity towards undesired product, indicating a complete diversion from the targeted reaction pathway. This observation contrasts with reports in literature highlighting the efficiency of Pd-Au catalysts in biomass-derived compound transformations, such as vanillin, under certain conditions [61]. The discrepancy might be attributed to differences in experimental setup, catalyst preparation, or reaction conditions. For instance, a study [42] demonstrated the effective use of Pd-Au bimetallic nanoparticles for vanillin HDO at room temperature with formic acid as the hydrogen donor, showcasing the potential for such catalysts in specific contexts. This could indicate that while Pd-Au combinations possess inherent catalytic qualities beneficial for HDO reactions, their performance depends on the reaction environment and parameters used in the experiments.

PdAg/TiO_2 and PdSn/TiO_2 exhibited moderate vanillin conversions of 23.2% and 8.4%, respectively, with a slight or null yield towards creosol of 1.2% and 0%, suggesting limited effectiveness in steering the reaction towards creosol production.

PdPt/TiO_2 catalyst demonstrated a significantly higher conversion rate of 99.2%, with a yield of 31.42% towards creosol and 67.8% towards undesired products. This catalyst

emerged as the most effective in promoting vanillin conversion while maintaining a substantial selectivity towards the desired product.

This behaviour could find some reasons in the work made by Liu et al. (2012) [62]. In this study it is reported that bimetallic Pd-Pt catalysts outperform monometallic Pd and Pt in benzofuran conversion and selectivity towards ethylcyclohexane, the HDO reaction product, under the same conditions. The article attributes this superior efficacy to increased metallic dispersion, enhancing accessible active sites. Alloying Pd with Pt is noted to promote surface segregation and uniform active site distribution, boosting activity. Furthermore, the introduction of Pt to Pd is described as generating new active sites with distinct properties and inducing structural changes, like Pd-Pd bond length adjustments and electronic density variations in the Pd valence band. These documented modifications from the Pd-Pt alloying process significantly elevate the catalysts' hydrogenation performance.

In our investigation, a direct enhancement in catalytic performance was not evident when comparing the bimetallic catalyst to its monometallic palladium counterpart under identical reaction conditions. Nonetheless, the superior performance of this specific bimetallic composition over other bimetallic combinations, coupled with supportive evidence from existing literature on this bimetal, has led us to further pursue research in this bimetallic system.

6.4 Metal ratio optimization

As Pd-Pt system was identified as the most promising one, a series of Pd-Pt bimetallic catalysts, varying metal ratios, were synthesized and tested in order to assess the impact of different Pd-Pt molar ratios on the catalytic efficiency of the HDO process. By adjusting the ratio of Pd to Pt in the catalyst's composition, the experiment aimed to explore the potential synergistic effects. The metal molar ratios explored were (Pd:Pt): 1:1, 3:1, 1:3, 4:1, 1:4 and both monometallic Pd and Pt.

For this part of the studies, the reaction time for all tests was maintained at 30 minutes. The other parameters remained consistent with previous tests: 3 atm of H_2, 300 rpm of magnetic stirring, 5 mL of vanillin solution at a concentration of 10 g/L, and 15 mg of

catalyst. The outcomes of the reactions are presented in the Table 13 and Figures 31 and 32.

Table 13. Resume of catalytic performances of Pd/Pt catalysts at different molar ratios

Me molar ratio	X% VAN	Y% CRE	Y% VAL	activity
Pd	14.41	3.38	11.03	82.54
Pd_4Pt_1	19.01	4.89	14.12	107.16
Pd_3Pt_1	100.00	16.45	82.46	725.42
PdPt	100.00	18.23	79.28	564.14
Pd_1Pt_3	11.24	2.12	9.12	59.62
Pd_1Pt_4	11.82	2.59	9.23	54.22
Pt	18.83	0.80	14.60	107.36

Reaction conditions: 20 °C, 3 atm H_2, 300 rpm, 5 mL of a 10 g/L VAN solution, 15 mg of catalyst, 30 min.

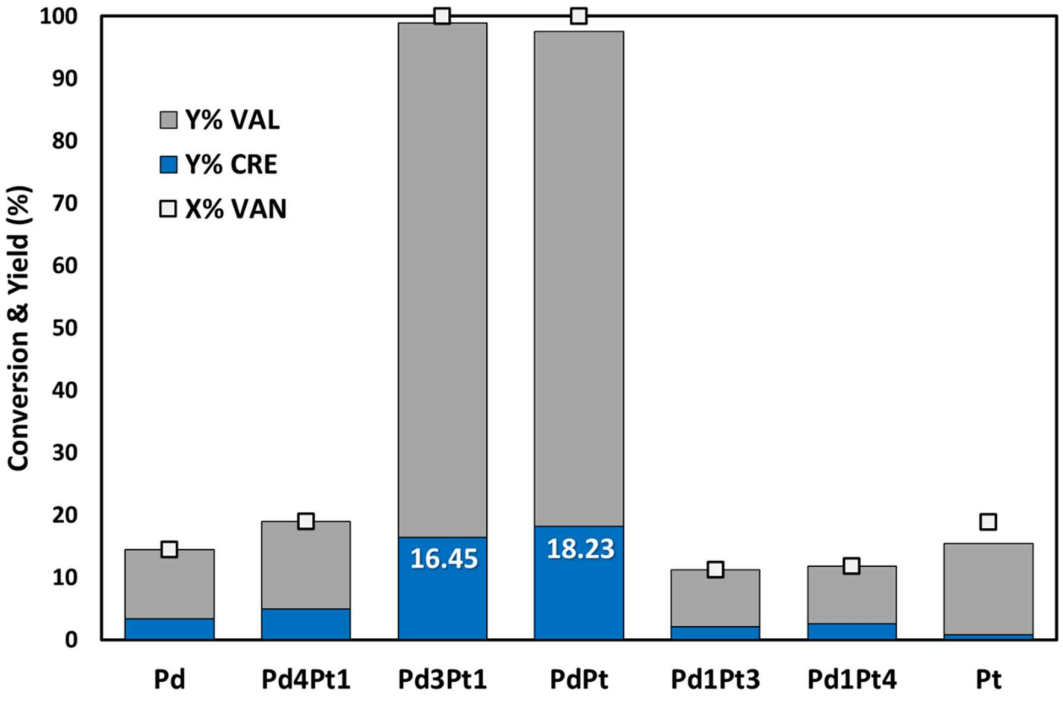

Figure 31. Catalytic performances of Pd/Pt catalysts at different molar ratios.

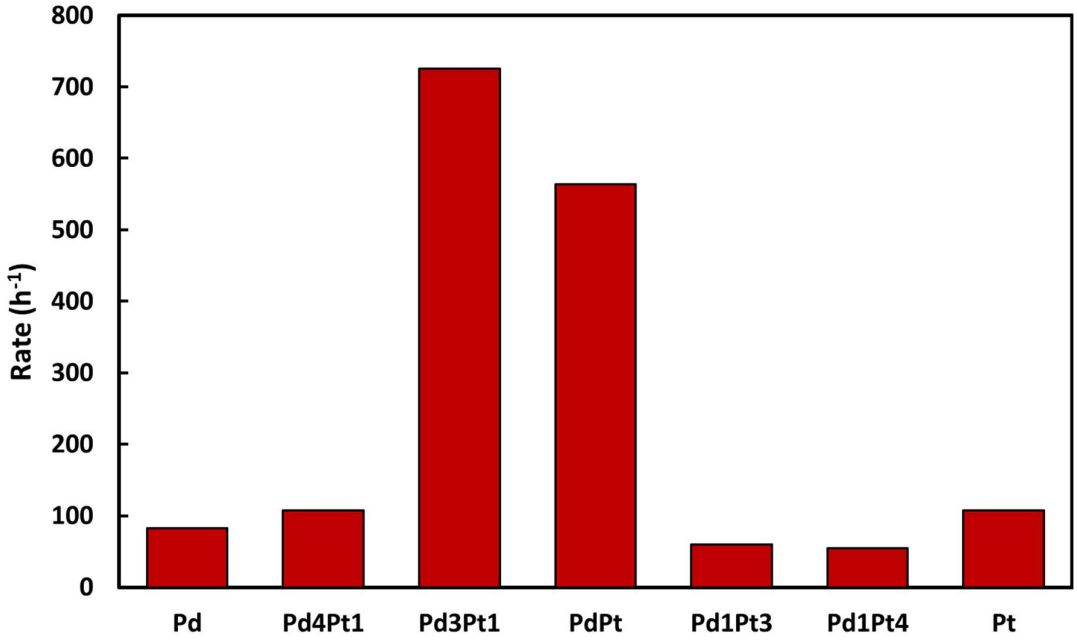

Figure 32. Catalytic activity of Pd-Pt bimetallic catalysts at different molar ratios.

The Pd_3Pt_1 and Pd_1Pt_1 ratios stand out significantly in the dataset, showcasing a profound effect on the catalytic process. The two catalysts achieved a 100% conversion rate of vanillin, with a selectivity of 16.4% and 18.23%, respectively for Pd_3Pt_1 and Pd_1Pt_1, towards creosol, mirroring the yield due to the complete conversion. Remarkably, the activity of this catalysts was measured at an impressive 725 h^{-1} for Pd_3Pt_1 and 587 h^{-1} for Pd_1Pt_1, far surpassing the activities observed with the Pd monometallic and other molar metal ratios at the same reaction conditions.

The substantially higher activity associated with the Pd_3Pt_1 and Pd_1Pt_1 ratio underscores the critical influence of a more balanced Pd to Pt ratio in optimizing the catalyst's performance. This enhanced activity can be attributed to an optimal synergistic interaction between Pd and Pt, which not only facilitates a more efficient hydrogenation and deoxygenation process but also significantly improves the catalytic system's overall efficacy.

6.5 Tests focused on Pd_3Pt_1

While both Pd_3Pt_1 and Pd_1Pt_1 catalysts' ratios exhibited high catalytic activity relative to other metal ratios tested, the activity of Pd_3Pt_1 was visibly superior to that of Pd_1Pt_1. This observation guided the focus of other catalytic performance tests towards the 3:1 ratio, in order to garner additional insights into its performance capabilities. These tests were carried out at 20°C and 50°C, with reaction times ranging from 0.5 to 4 hours. The other reaction parameters were: 3 atm of H_2, 300 rpm of magnetic stirring, 5 mL of vanillin solution at a concentration of 10 g/L, and 15 mg of catalyst. The outcomes of the reactions are presented in the table 14 and Figures 33 and 34 below.

Table 14. resume of Pd_3Pt_1/TiO_2 reactions outcomes varying temperature and reaction time.

T (°C)	t (h)	X% VAN	Y% CRE	Y% VAL
20.00	0.50	100.00	16.45	82.46
20.00	1.00	100.00	59.11	39.86
50.00	0.50	100.00	43.72	53.15
50.00	1.00	100.00	76.62	19.87
50.00	2.00	100.00	95.08	3.21
50.00	4.00	100.00	100.00	0.00

Reaction conditions: 300 rpm, 3 atm H_2, 5 mL of a 10 g/L VAN solution, 15 mg of catalyst.

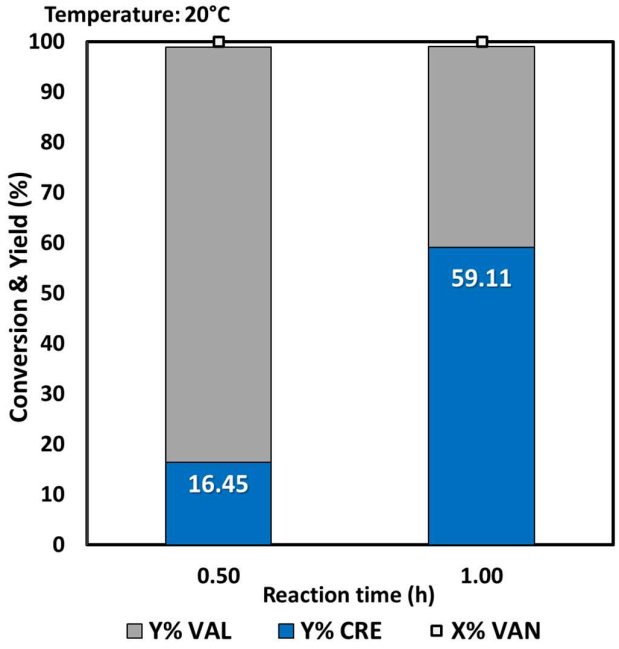

Figure 33. Pd_3Pt_1/TiO_2 catalytic performance at 20°C in 20 min and 1h of reaction time.

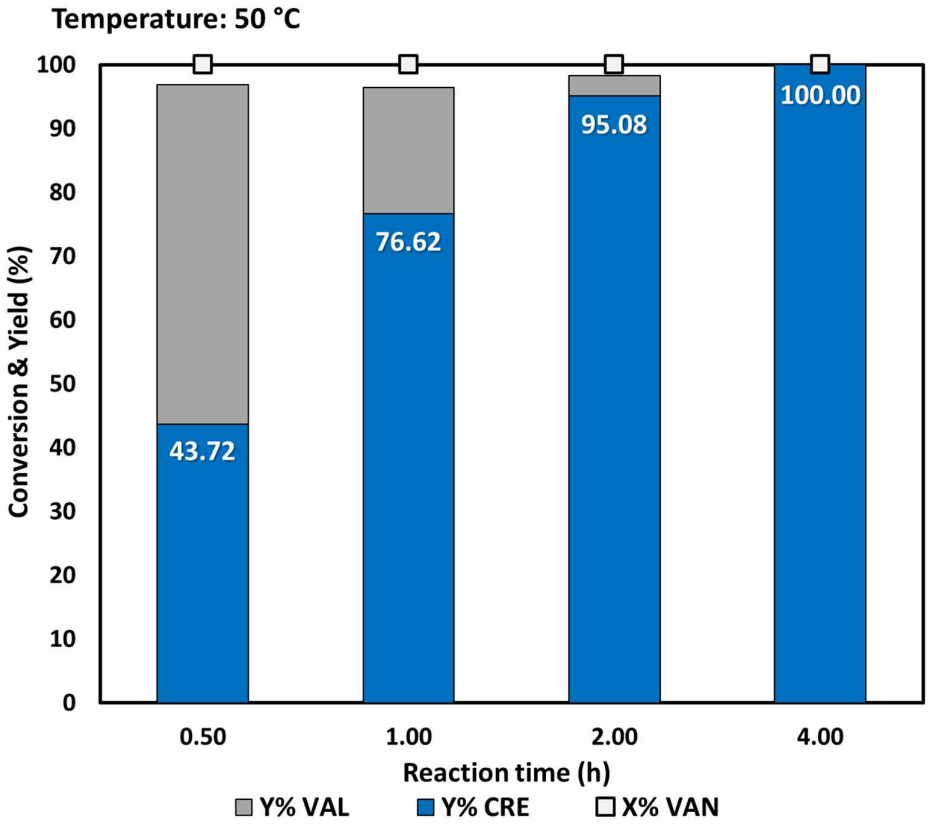

Figure 34. Pd_3Pt_1/TiO_2 catalytic performances varying the reaction time at 50 °C.

At 20°C for 0.5 hours, as shown before, the conversion was complete (100%), with a selectivity of 16.45% towards creosol. Extending the time to 1 hour at 20 °C significantly shifted selectivity towards creosol to 59.11%, suggesting increased effectiveness for creosol production with longer exposure. At 50 °C for 0.5 hours, selectivity for creosol was 43.72%, showing temperature's role in enhancing deoxygenation. Increasing time to 1 hour at 50 °C further enhanced creosol selectivity to 76.62%, indicating a potential optimal point for creosol production. Further extending the time to 2 and 4 hours at 50 °C resulted in nearly exclusive selectivity towards creosol (95.08% and 100%, respectively).

6.6 Tests on Niobium Oxide

In Section 6.3, it is demonstrated that a monometallic Pd catalyst supported on Nb_2O_5 could achieve a selectivity towards creosol of over 40%, thereby garnering interest in the exploration of niobium oxide (Nb_2O_5) as a support material for the optimal

bimetallic Pd_3Pt_1 catalyst. This segment of the study aimed to assess the impact of Nb_2O_5 as a catalyst support, investigating its effect on catalytic performance. The selection of this support material was informed by its previously discussed intrinsic acidity, which is posited to enhance the hydrodeoxygenation (HDO) reaction.

Thus, Pd_3Pt_1/Nb_2O_5 was synthesized with the same sol-immobilization preparation method and subsequently tested at room temperature and at different reaction time. The other parameters remained consistent with previous tests: 3 atm of H_2, 300 rpm of magnetic stirring, 5 mL of vanillin solution at a concentration of 10 g/L, and 15 mg of catalyst. The outcomes of the reactions are presented in the table 15 and Figure 35.

Table 15. Resume of catalytic outcomes in HDO of vanillin using Pd_3Pt_1/Nb_2O_5 varying the reaction time.

Reaction time (h)	X% VAN	Y% CRE	Y% VAL
0.25	34.92	5.197	29.73
0.5	70.86	9.16	61.71
1	100	47.59	51.27

Reaction conditions: 20 °C, 300 rpm, 3 atm H_2, 5 mL of a 10 g/L VAN solution, 15 mg of catalyst.

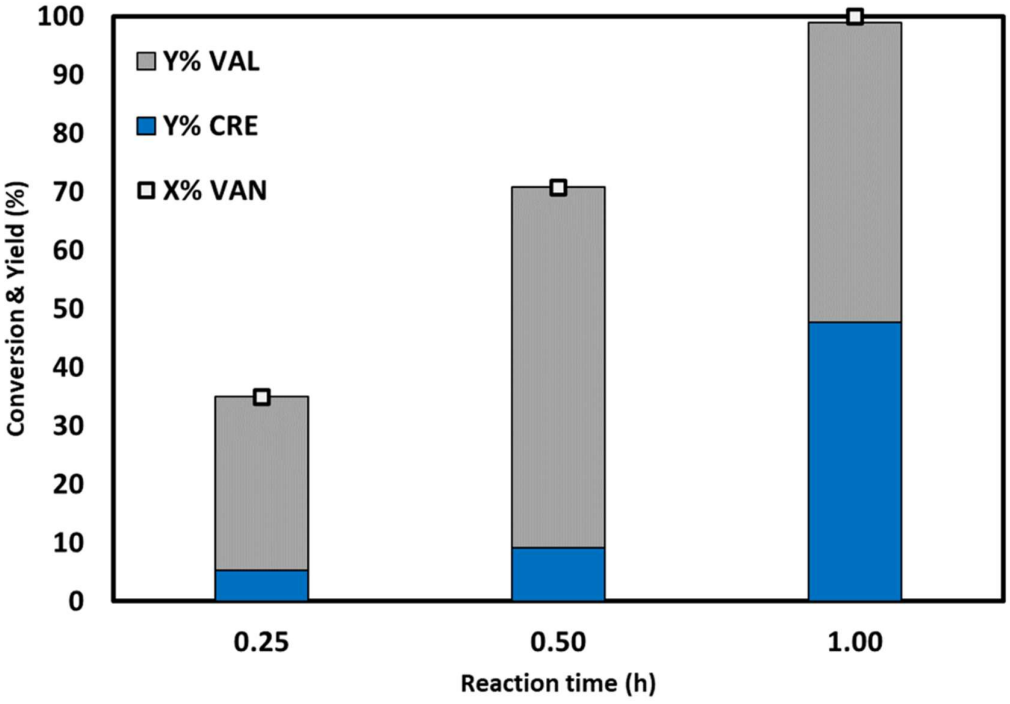

Figure 35. Catalytic performances of Pd_3Pt_1/Nb_2O_5 catalyst varying reaction time.

The catalyst demonstrated very good catalytic performance. Even after 15 minutes of reaction time, it could convert a significant amount of vanillin into creosol, proving to be an effective catalyst for facilitating the Hydrodeoxygenation (HDO) step even under mild reaction conditions. However, compared to Pd_3Pt_1/TiO_2, the latter showed a higher production of CRE both after 30 minutes and 1 hour of reaction time (figure chapter before). Further comparisons were made between the before mentioned catalyst and the monometallic Pd/Nb_2O_5 catalyst, which were also tested at 20 °C and 80°C with a reaction time of 1 hour (Figure 36). Both Pd/Nb_2O_5 and Pd_3Pt_1/Nb_2O_5 achieved 100% vanillin conversion.

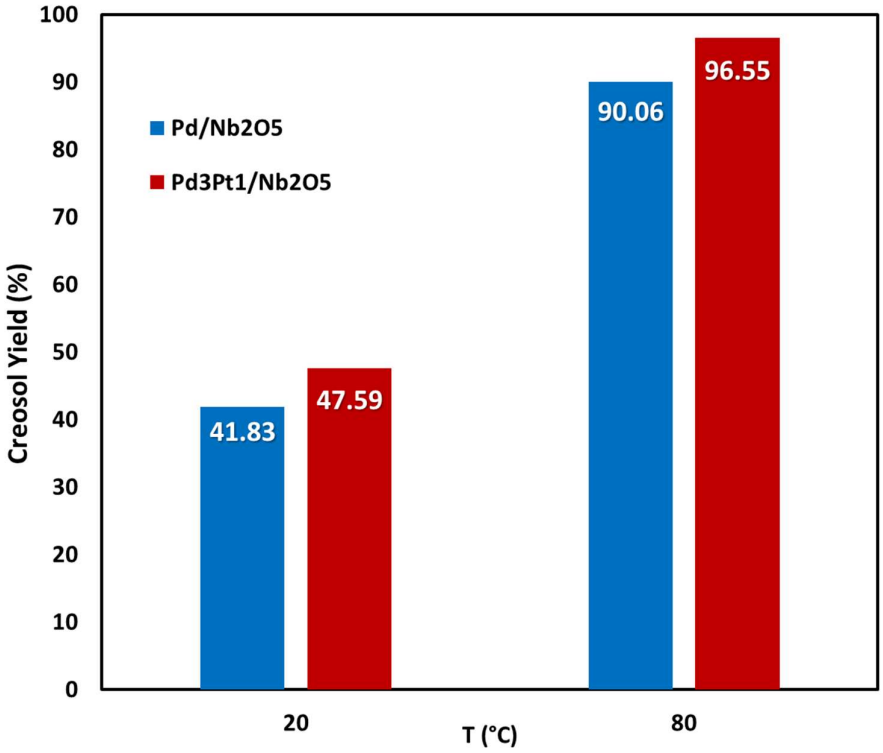

Figure 36. Comparisons between the catalytic performances at 20 °C and 80 °C of monometallic and bimetallic catalysts using Nb_2O_5 as support.

The results suggest that a positive synergy between palladium and platinum is also established when using Nb_2O_5 as the catalyst. The outcomes at 20 °C, compared to the same reaction conditions in tests with Pd_3Pt_1/TiO_2 and the monometallic Pd/TiO_2, demonstrate that on the TiO_2 support, the presence of platinum leads to a superior improvement in performance compared to the improvement observed with Nb_2O_5 (Figure 37).

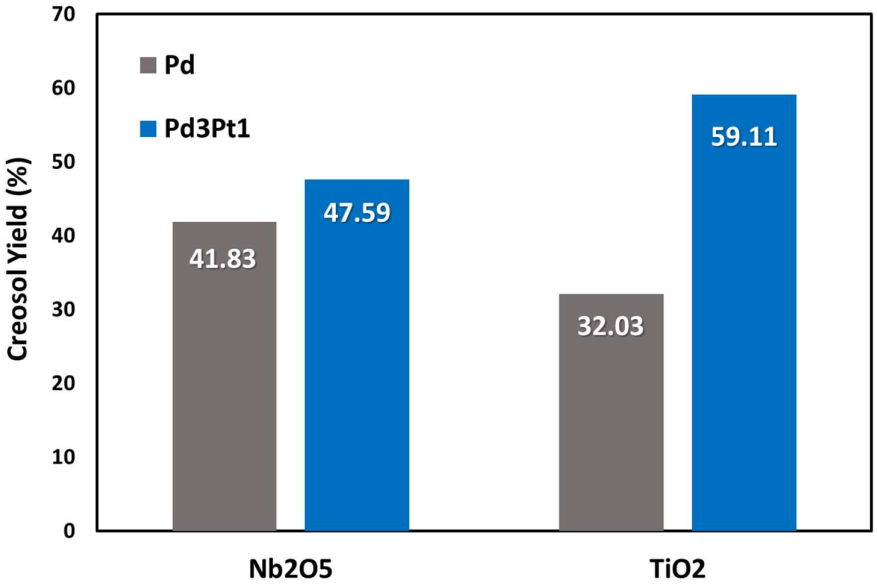

Figure 37. Comparisons between TiO_2 and Nb_2O_5 support in bimetallic Pd_3Pt_1 and monometallic Pd catalysts.

A by-product: Vanillyl isopropyl ether

During the characterization of the reaction products, an uncharacteristic peak, not recognizable through the molecule recognition function of the MS software, was observed in some tests. The retention time of this compound was measured at approximately 20.7 minutes, and its corresponding MS spectrum is reported in Figure 38.

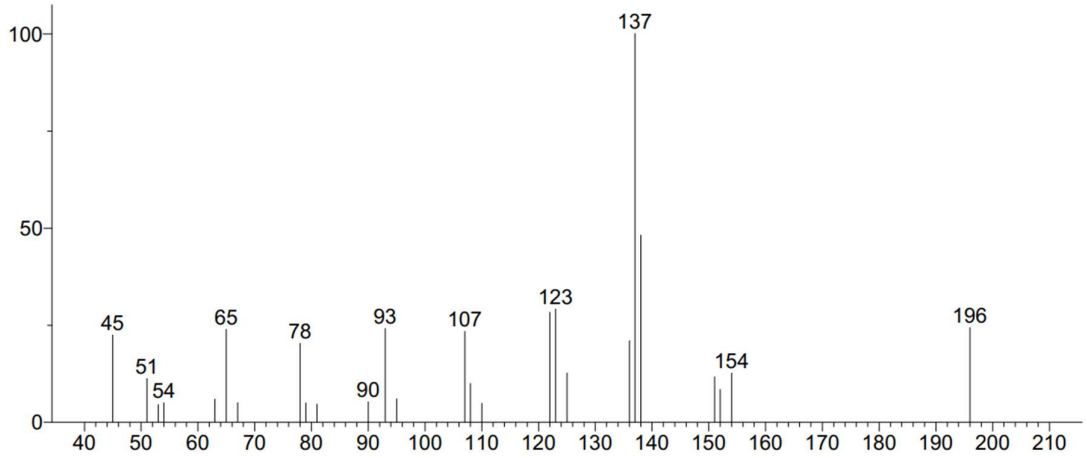

Figure 38. MS spectra of the compound

In the study by [63] where reaction conditions were comparable to those described in this thesis, a byproduct was identified. This byproduct originated from the parasitic condensation reaction between two alcohols present in the reaction environment: the initial reaction product, VAL, and the solvent, isopropanol. These compounds in the reaction environment facilitated the condensation reaction, leading to the formation of vanillyl isopropyl ether (VIE). The aforementioned study proposed a reaction network starting from vanillin that includes this secondary reaction, as depicted in Figure 39.

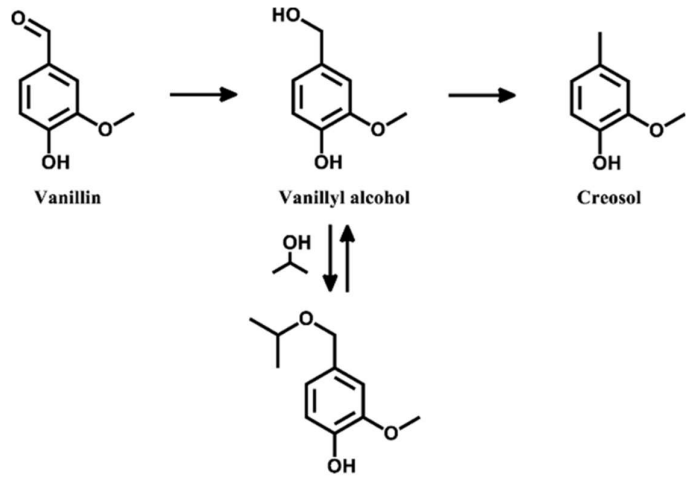

Figure 39. Pathway considering the vanillyl isopropyl ether formation.

The emergence of this peak always exhibited an area on the FID instrument often too low to be considered a competitive co-product for the reaction of interest. Therefore, it was not extensively investigated, and insufficient data were collected to identify a correlation between the presence of this compound and any reaction parameter or reactant presence. Compared to the findings in the cited study, where the ether's presence was noted in most experiments, in this work, its presence was identified in a rare number of reactions and always in trace amounts. This led to the decision to exclude the compound from quantitative calculations.

7 RESULT AND DISCUSSION II - CATALYSTS CHARACTERIZATION

7.1 ICP-OES

The catalytic results presented above shoved high efficiency of Pd-Pt/TiO_2 catalysts on HDO of vanillin. The catalytic activity was strongly influenced by the Pd to Pt molar ratio. Compositional analysis conducted via ICP-OES on the synthesized bimetallic and monometallic platinum and palladium catalysts indicates a commendable alignment with theoretical values, underscoring the precision of the sol-immobilization method for the array of catalysts (Table 2). For instance, the Pd_4Pt_1 catalyst achieved an actual Pd:Pt ratio of 3.96, closely approximating the theoretical target of 4, and the PdPt catalyst displayed a ratio of 1.05, slightly over the aimed parity. An exception was observed in the Pd_3Pt_1 catalyst, which exhibited a ratio of 3.79, diverging from the expected ratio of 3. This variance, while notable, does not detract from the overall success of the synthesis process but rather highlights the complexities inherent in achieving precise bimetallic ratios. The data still suggest that the employed synthesis method can produce catalysts with near-target compositions, which is critical for optimizing catalytic performance for specific reactions.

Table 16. ICP analysis results of mono- and bimetallic catalysts.

Catalyst	% $Pd_{theoric}$	% Pd	% $Pt_{theoric}$	% Pt	% metal	Pd:$Pt_{theoric}$	Pd:Pt
Pd	1	0.96	0	0	0.96		
Pd_4Pt_1	0.69	0.67	0.31	0.31	0.98	4	3.96
Pd_3Pt_1	0.62	0.60	0.38	0.29	0.91	3	3.79
PdPt	0.35	0.23	0.65	0.4	0.63	1	1.05
Pd_1Pt_3	0.21	0.16	0.85	0.72	0.88	0.33	0.41
Pd_1Pt_4	0.15	0.13	0.88	0.81	0.94	0.25	0.29
Pt	0	0	1	0.98	0.98		

7.2 X-ray Diffraction (XRD)

X-ray diffraction analysis (XRD) was conducted to determine the crystalline phases present in the two most active catalysts Pd_3Pt_1 and Pd_1Pt_1, and both monometallic.

Notably, diffraction peaks corresponding to Pd and Pt were absent (Figure 40), indicating the highly dispersed nature of these metals on the support or their incorporation into the TiO_2 lattice at concentrations below the detection limit of XRD. Furthermore, the analysis revealed the presence of both anatase and rutile phases of TiO_2, respectively 25° and 27.5° approximately, with the rutile phase constituting around 5% of the total TiO_2 structure, indicates the presence of these crystalline structures.

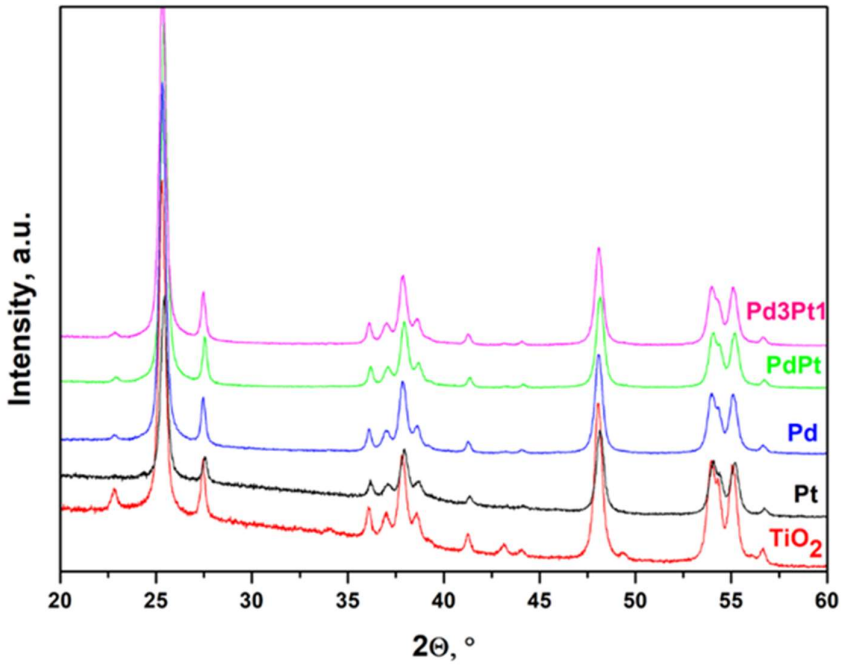

Figure 40. XRD patterns of mono and bimetallic Pd-Pt/TiO2 catalysts

The X-ray Diffraction (XRD) analysis presented here provides indirectly key insights into the dispersion of Pd and Pt on the TiO_2 support. The absence of distinct diffraction peaks corresponding to Pd and Pt suggests that these metals may be highly dispersed on the support. Typically, XRD is capable of detecting particles with a minimum crystallite size in the range of several nanometers; therefore, the lack of Pd and Pt peaks indicates that the particle sizes are below this detection threshold.

Furthermore, the consistency of the diffraction peaks across all catalyst samples, despite varying Pd to Pt ratios, corroborates that the metal particles remain below the detection limit of the XRD instrument in all cases. This uniform absence of metallic peaks across

different catalyst compositions strongly suggests that the metals are finely dispersed, and there is no significant agglomeration that would lead to particle sizes within the detectable range. This high degree of metal dispersion is desirable in catalysis, as it maximizes the surface area available for the catalytic reactions, potentially leading to enhanced catalytic activity. The XRD data, therefore, hint at a successful preparation of catalysts with metals in a highly dispersed state, a condition that is typically associated with improved catalytic performance.

7.3 TEM: Morphological Analysis

Transmission Electron Microscopy (TEM) was employed to investigate the morphology and size distribution of Pd-Pt nanoparticles on the catalyst supports. TEM analyses were conducted on monometallic and on the Pd_1Pt_1, Pd_3Pt_1 and Pd_1Pt_3 bimetallic catalysts. Images obtained are presented on Figure 41.

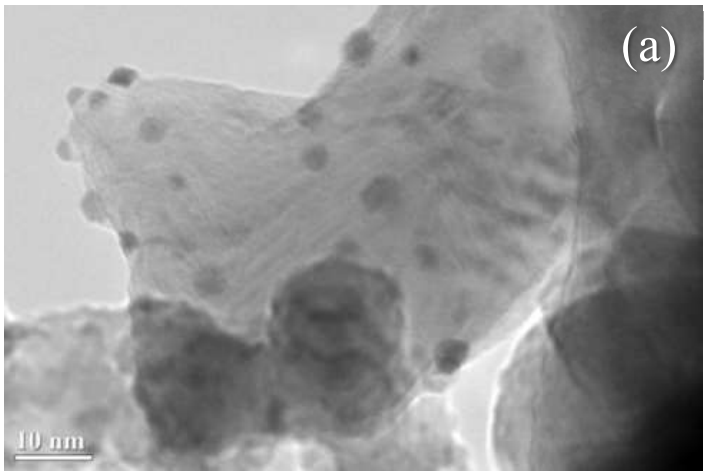

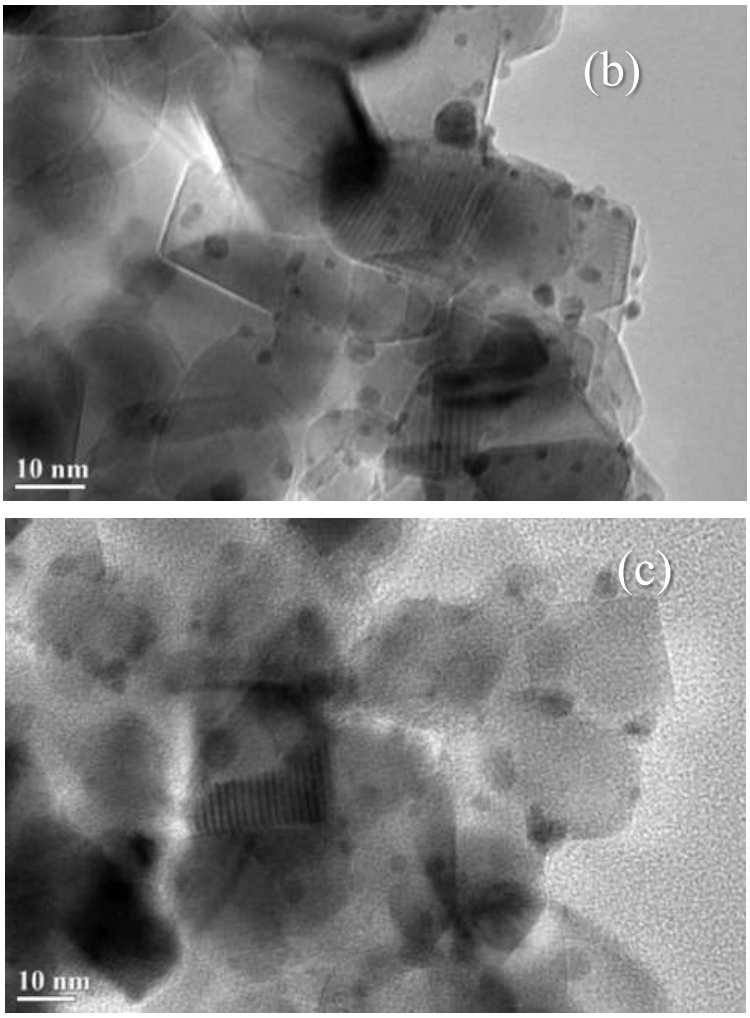

Figura 41. TEM images of the a) PdPt, b) Pd_3Pt_1 and c) Pd_1Pt_3 catalysts.

The TEM images served as a foundational tool for understanding the dispersion and interaction of Pd particles with the support material. TEM analysis revealed that Pd and Pd-Pt particles were uniformly distributed on the TiO_2 surface with a narrow particle size distribution.

7.4 STEM & HAADF

Due to any notable difference observed in particle size or distribution, a special attention was paid to the formation of nanoalloys between Pd and Pt in the particles. STEM and HAADF-STEM analyses offered complementary perspectives on the catalysts' nanostructure. HAADF-STEM analysis was performed on Pd_3Pt_1, Pd_1Pt_1 and Pd_1Pt_3 bimetallic catalysts (Figures 42, 43 and 44).

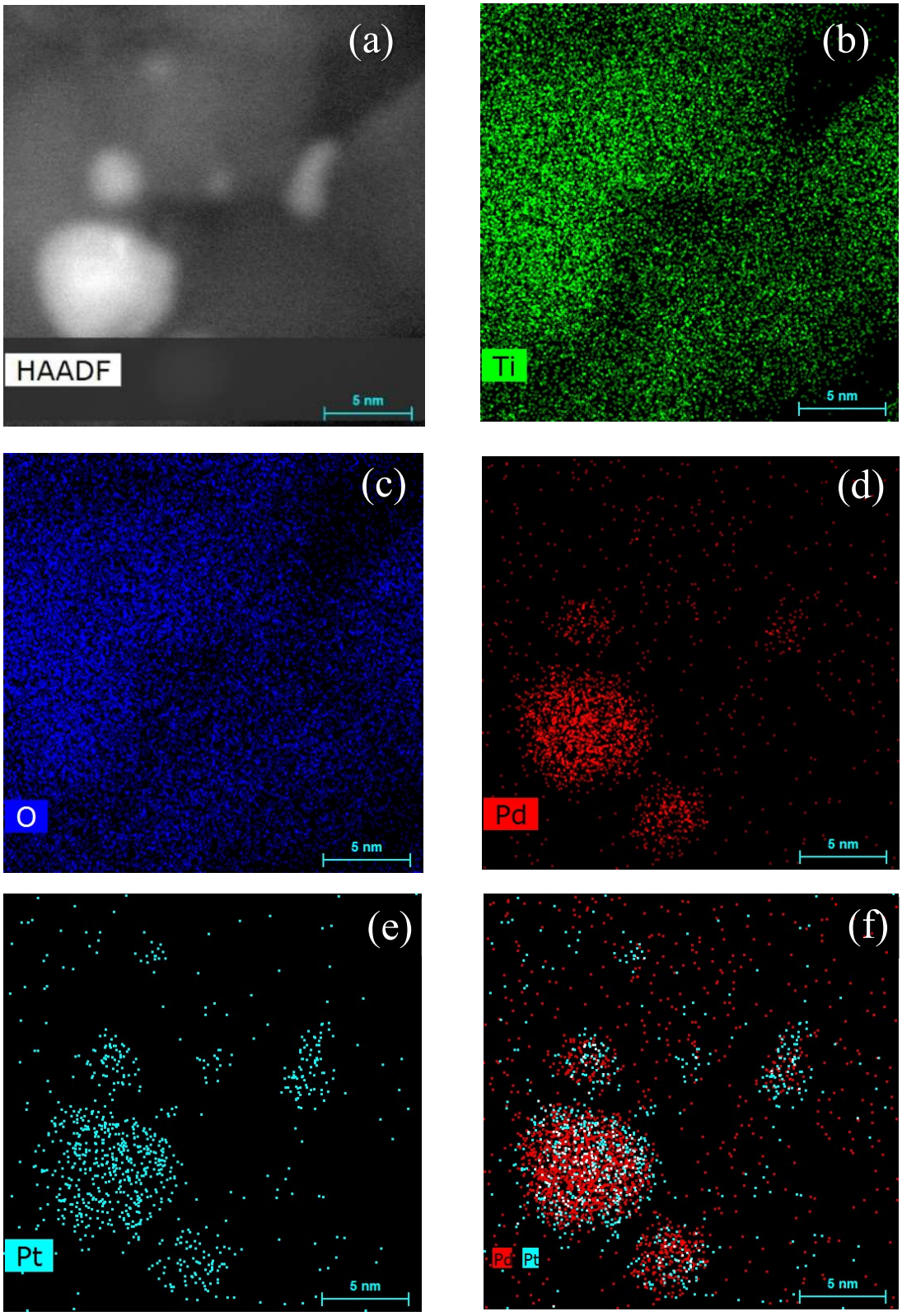

Figure 42. HAADF-STEM and EDX-mapping of Pd1Pt1 catalyst: HAADF image of analysed region (a), Ti (b), O (c), Pd (d), Pt (e), and Pd / Pt (f).

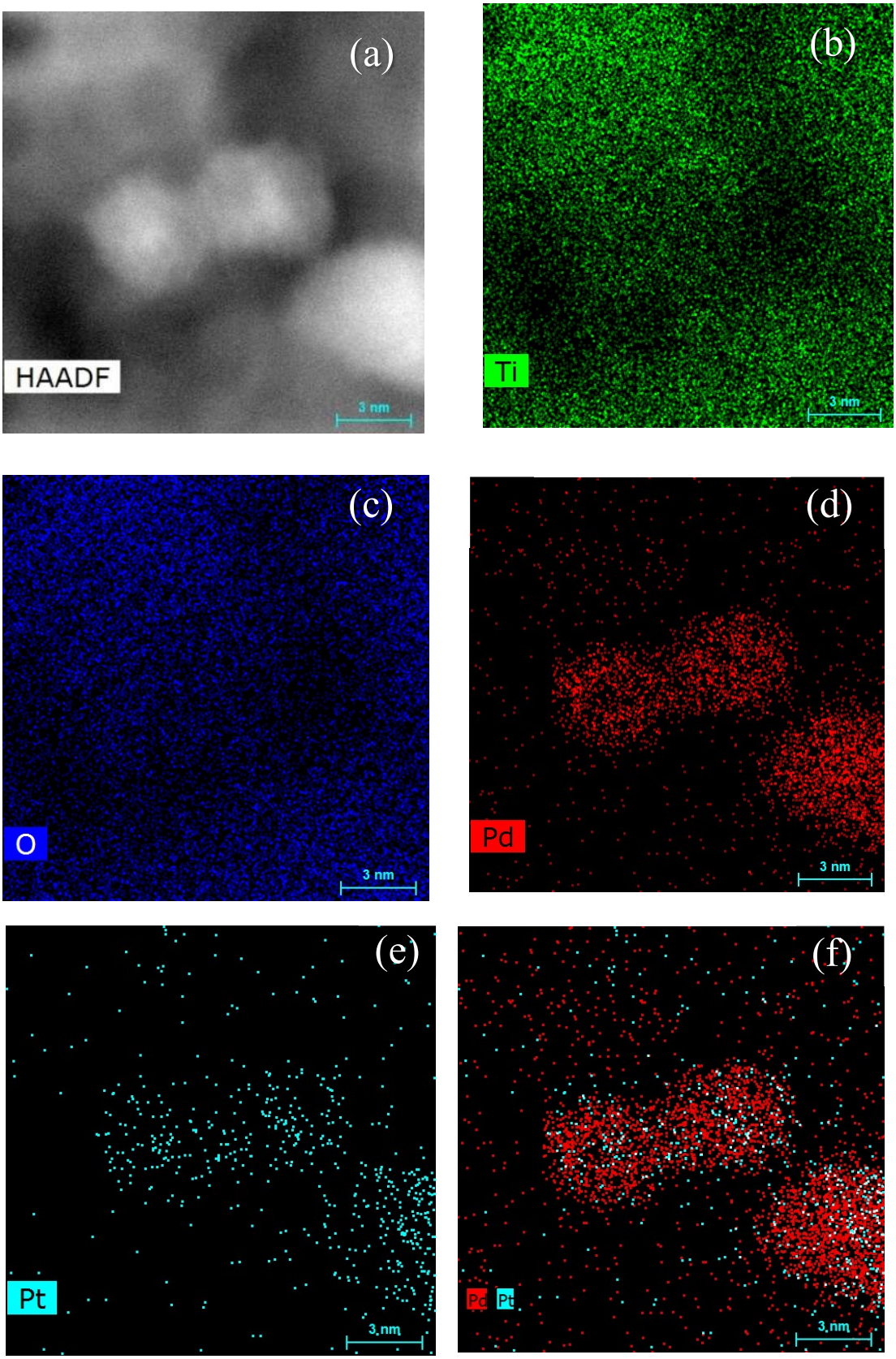

Figure 43. HAADF-STEM and EDX-mapping of Pd_3Pt_1 catalyst HAADF image of the analysed region (a), Ti (b), O (c): Pd (d), Pt (e), and Pd / Pt (f).

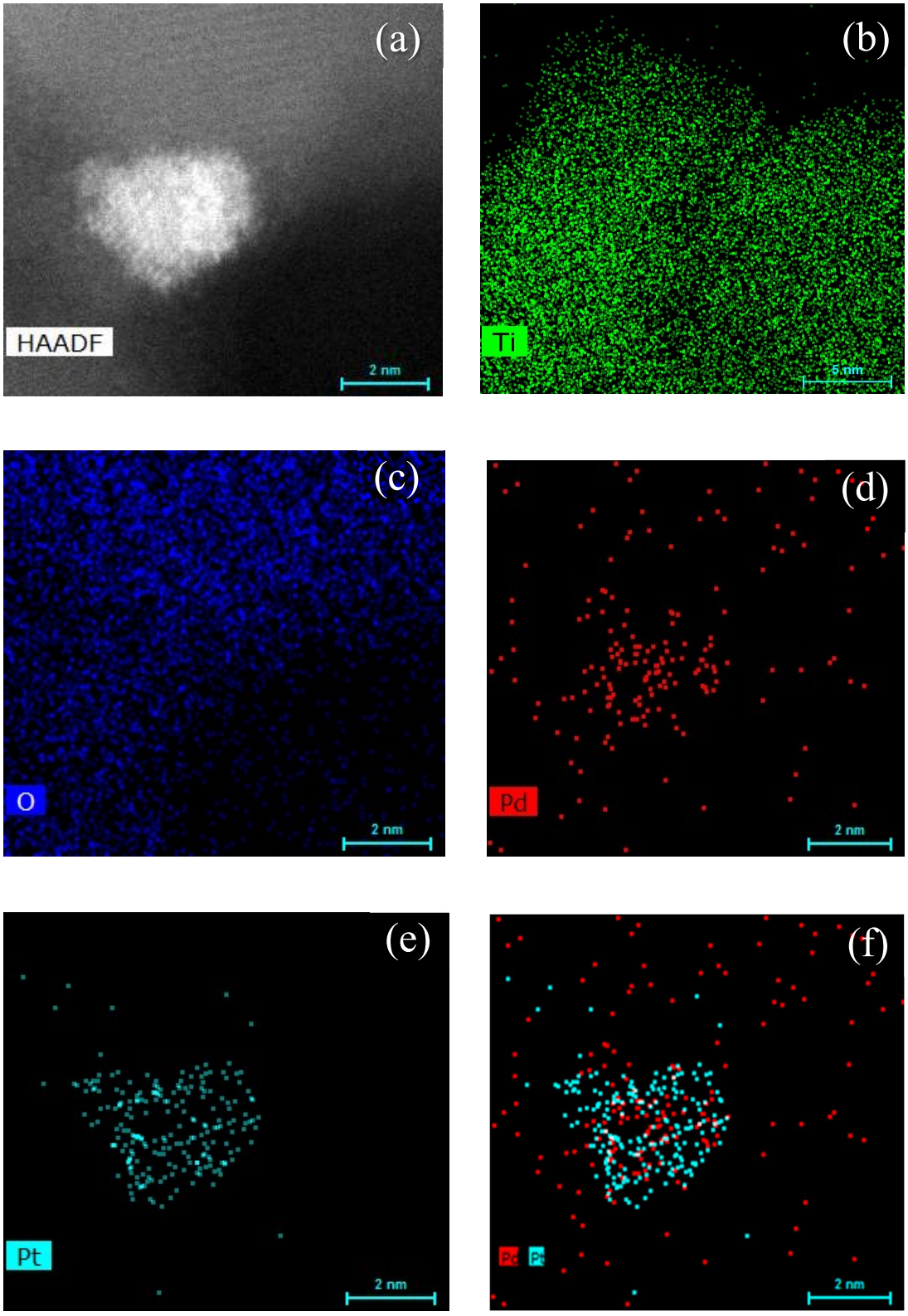

Figure 44. HAADF-STEM and EDX-mapping of Pd_1Pt_3 catalyst: HAADF image of analysed region (a), Ti (b), O (c), Pd (d), Pt (e), and Pd / Pt (f).

No segregation was detected, indicating the formation of random Pd-Pt nanoalloys, consistent with previous studies. In fact, in the study outlined by Ferrando et al. [45], where the formation of nanoalloys without segregation, leading to nanoalloy formation, extensively analysed it's highlighted that the intimate mixing of metals in nanoalloys is influenced by various factors, such as the relative bond strength between different metals, their surface energy, atomic sizes, charge transfer dynamics, and the role of stabilizer ligands. It is reported that when the alloy bond strength surpasses that of the constituent pure metals, a homogeneous mixture is favoured over segregation. This principle is crucial for the synthesis of nanoalloys, where metals are mixed in an atomically ordered or randomly dispersed manner, avoiding segregated structures. The EDX-mapping images obtained from the analysis showed that both metals are homogeneously distributed, and that the Pt is localized mostly on the surface of the bimetallic particles. This uniform size distribution and the absence of segregation indicate a successful alloying process between Pd and Pt, leading to the formation of nanoalloys with potentially enhanced catalytic properties. Furthermore, the consistency of the nanoparticle size across different samples suggests a controlled synthesis process, ensuring that the nanoparticle ratio of the two metals adheres to the proportions identified by Inductively Coupled Plasma (ICP) analysis. The merging of the two metals into a single nanoparticle entity, coupled with their well-dispersed nature on the support, is indicative of a synthesis approach that effectively combines Pd and Pt to harness the synergistic effects of bimetallic catalysis.

7.5 ICP-OES RESULTS vs CATALYTIC PERFORMANCES

ICP-OES analysis determined the percentage weight of metals in each bimetallic catalyst, varying by ratio. This data allows for comparison with previously reported performance metrics to identify potential correlations between catalyst efficacy and specific metal content. Given that ICP-OES provides metal content as a percentage of the total sample and the total metal content varies across catalysts, a normalized value (NV) was calculated as follows:

$$\mathrm{NV} = \frac{wt\%\ of\ specific\ metal}{wt\%\ sum\ of\ both\ metals}$$

This normalization allows for a more accurate comparison across different catalyst compositions by adjusting for the total metal content. Focusing on Palladium, the calculated values are represented in table. Then, the normalized values of each catalyst have been plotted with the corresponsive catalysis metrics for have a direct visual view of the effect of the real Palladium on the reactions.

Table 17. Normalized values calculation of different ratios Pd-Pt catalysts.

catalyst	%wt Pd	% wt metals sum	NV
Pd	0.96	0.96	1
Pd_4Pt_1	0.67	0.98	0.68
Pd_3Pt_1	0.60	0.91	0.66
PdPt	0.23	0.63	0.37
Pd_1Pt_3	0.16	0.88	0.18
Pd_1Pt_4	0.13	0.94	0.14
Pt	0	0.98	0

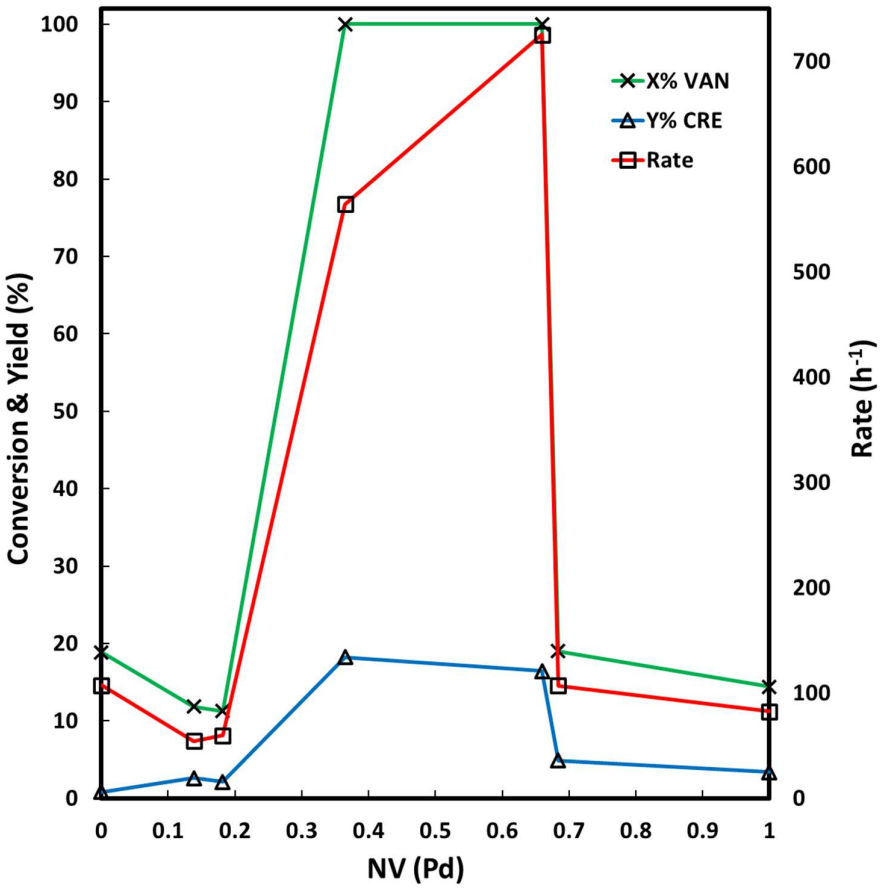

Figure 45. Correlation between catalytic performances and the normalized Pd bulk content (from ICP) in bimetallic catalysts.

The analysis yielded intriguing findings. A good volcano like correlation was observed (Figure 45). The results indicate that catalytic performances strongly depend on the Pd to (Pd+Pt) ratio. Furthermore, a region is identified where the considered catalytic properties are significantly enhanced: between values of 0.2 and 0.7, corresponding to 20% and 70% of Pd weight content relative to the total metal weight. Outside this range, under the tested reaction conditions, catalytic performances markedly decline. Compared to the theoretical percentages expected for the catalysts (Table 2), the range just described is broader: the span exhibiting heightened catalytic activity extends over than 50% of the value spectrum. Moreover, the domain of peak catalytic performance is defined by only two data points. This makes challenging to precisely determine the optimal percentage range for the two metals.

7.6 XPS RESULTS

Because ICP is a bulk technique, and all the catalysis dynamics occurs at the surface of active sites, it has been decided also to check if the correlation between surface composition and catalytic performance is also present in the case of metals surface compositions. XPS analysis, as a surface sensitive technique was performed on monometallic, Pd_3Pt_1, PdPt and Pd_1Pt_3 catalysts. The results are given in Table 18 and figures 46, 47, 48 and 49.

Table 18. XPS results for mono and bimetallic Pd-Pt catalysts from Pd 3d and Pt 4f regions.

Catalyst	Pd %	Pt %	$Pd^0/(Pd^0+Pt^0)$	Pd/Pt	Pd/Ti	Pt/Ti	BE eV
Pd/TiO_2	0.14	-	1	-	0.059	-	$Pd_{5/2}$ – 335.12
Pd_3Pt_1	0.12	0.04	0.75	3.00	0.037	0.012	$Pd_{5/2}$ – 335.19 $Pt_{7/2}$ – 71.07
PdPt	0.10	0.08	0.55	1.25	0.022	0.018	$Pd_{5/2}$ – 335,02 $Pt_{7/2}$ – 70.58
Pd_1Pt_3	0.05	0.14	0.26	0.36	0.013	0.036	$Pd_{5/2}$ – 334,63 $Pt_{7/2}$ – 70.22
Pt/TiO_2	-	0.08	0	-	-	0.035	$Pt_{7/2}$ – 70.00

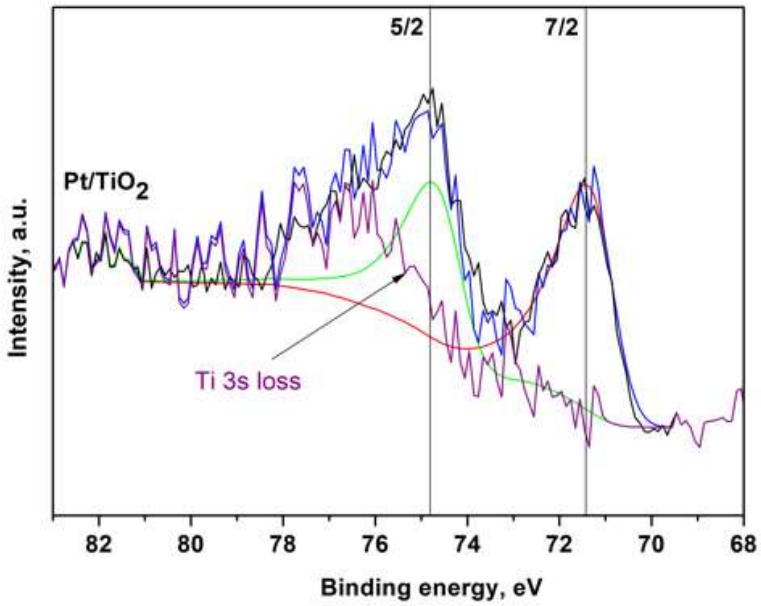

Figure 46. Pt/TiO_2 XPS spectra in Pt 4f region.

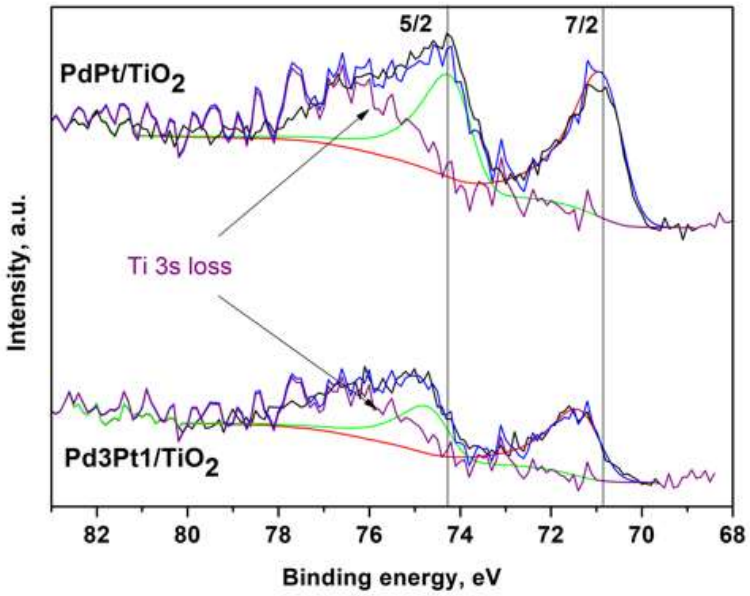

Figure 47. $PdPt/TiO_2$ and Pd_3Pt_1/TiO_2 XPS spectra in Pt 4f region.

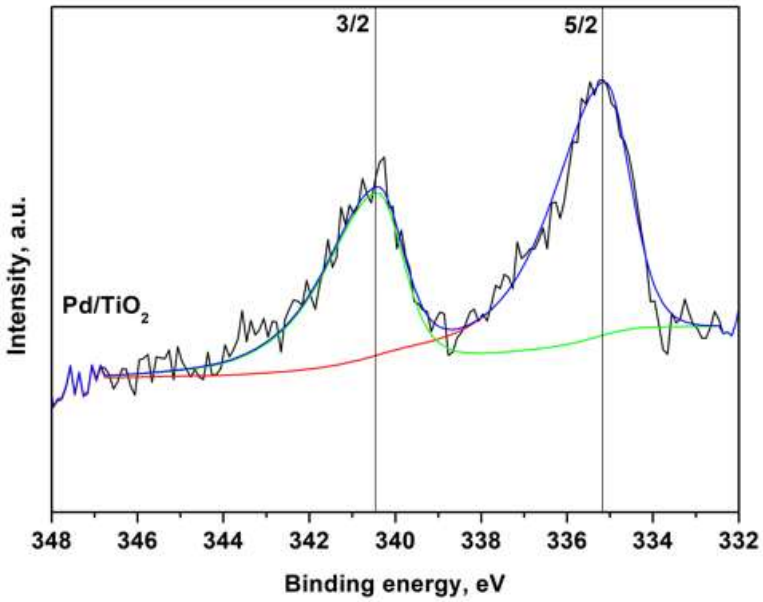

Figure 48. Pd/TiO_2 XPS spectra in Pd 3d region

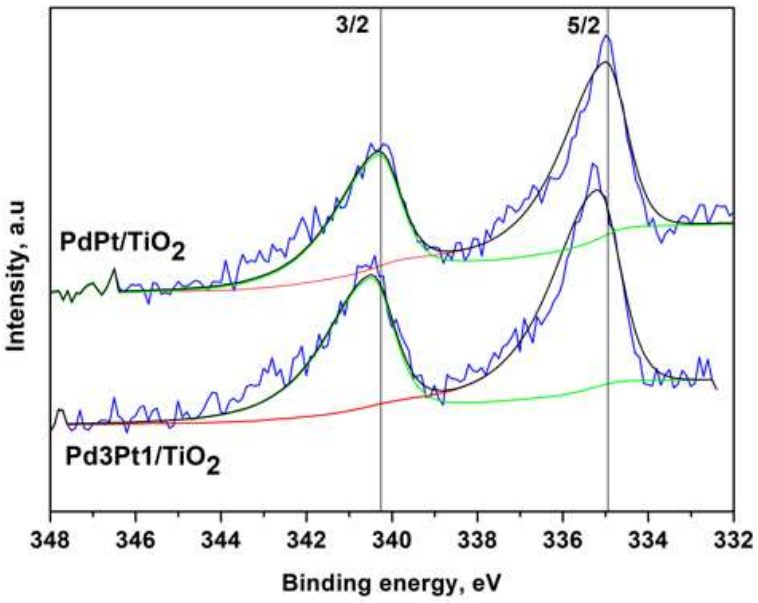

Figure 49. Pd_1Pt_1/TiO_2 and Pd_3Pt_1/TiO_2 XPS spectra in Pd 3d region.

To comprehend these graphs, it is crucial to recognize the components of the spectra and their respective implications. Firstly, the red and green lines represent theoretical peak positions and shapes, as derived from tabulated data. These lines are smooth, lacking oscillations, as they are based on calculations grounded in established theoretical frameworks. They serve as a reference, allowing us to anticipate the binding energy positions for specific electronic states of the elements present. The black lines

overlaying the spectra denote the experimental reference data, which is also tabulated but based on empirical evidence. These lines indicate the expected instrument response under ideal conditions. Our primary focus lies on the blue lines, which delineate the actual experimental data obtained from the analysis of the synthesized catalysts. The peaks and troughs in these lines reflect the real-world interaction of X-rays with the material, revealing the binding energies of electrons within the sample. Lastly, the purple line signifies the contribution from the support material, TiO_2, showing its characteristic loss features and providing context for the catalyst peaks. In interpreting these graphs, one aligns the experimental data (blue line) with both the theoretical (red and green lines) and empirical experimental (black line) spectra. This alignment allows for an assessment of how closely the actual material behaviour reflects theoretical expectations and known empirical data. Discrepancies can yield insights into the nature of the surface, including the electronic environment of the adsorbed species and the potential for chemical shifts indicative of interaction between the metal particles and the support.

Understood this, XPS analysis was also performed in order to assess the oxidation states of Pd and Pt on the surface of the catalysts. The XPS data confirmed the presence only of metallic Pd and Pt on the surface of the catalysts for all samples. For the bimetallic Pd-Pt/TiO_2 catalysts, the Pd $3d_{5/2}$ peak was assigned to the metallic state of palladium, without evidence of peaks for Pd^{2+}, which would be expected at higher binding energies. Furthermore, in the Pt $4f_{7/2}$ region only one contribution was observed and it was attributed to Pt^0.

The XPS spectra reveal a discernible shift toward lower binding energies for the Pt $4f_{7/2}$ peak in the bimetallic samples when compared to monometallic counterparts. Similarly, modest but observable shifts were observed in the Pd $3d_{5/2}$ peak, particularly pronounced in the Pd_3Pt_1 catalyst. These shifts are indicative of an electronic modification of the Pt surface atoms, presumably through interaction with Pd. Such a shifting pattern aligns with the findings reported by Tang et al. (2018) in their work [64], wherein metallic peaks in Pd-Pt bimetallic catalysts deviated from the expected tabulated values. They reported a correlation between the palladium content in the

catalyst and the extent of peak shifting, affecting both Pt and Pd peaks as illustrated in figure 50.

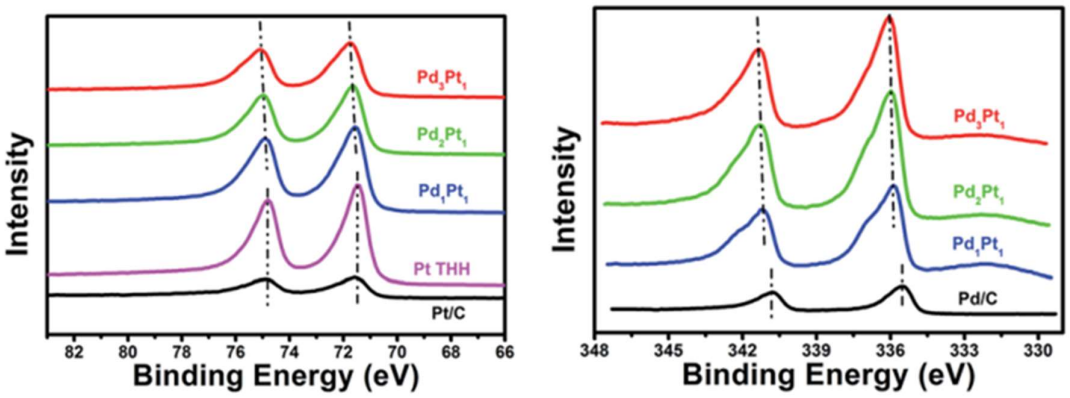

Figure 50. XPS peaks shifts in Pd-Pt bimetallic catalyst varying with metal molar ratio.

These observed shifts suggest a modification in the electronic structure of the catalysts, potentially affirming its significance in catalytic performances enhancement. The analysis of XPS and catalytic results has provided insightful findings regarding the dependence of catalytic activity and performances on the ratio of metallic Pd to the sum of metallic Pd and metallic Pt in bimetallic Pd-Pt catalysts.

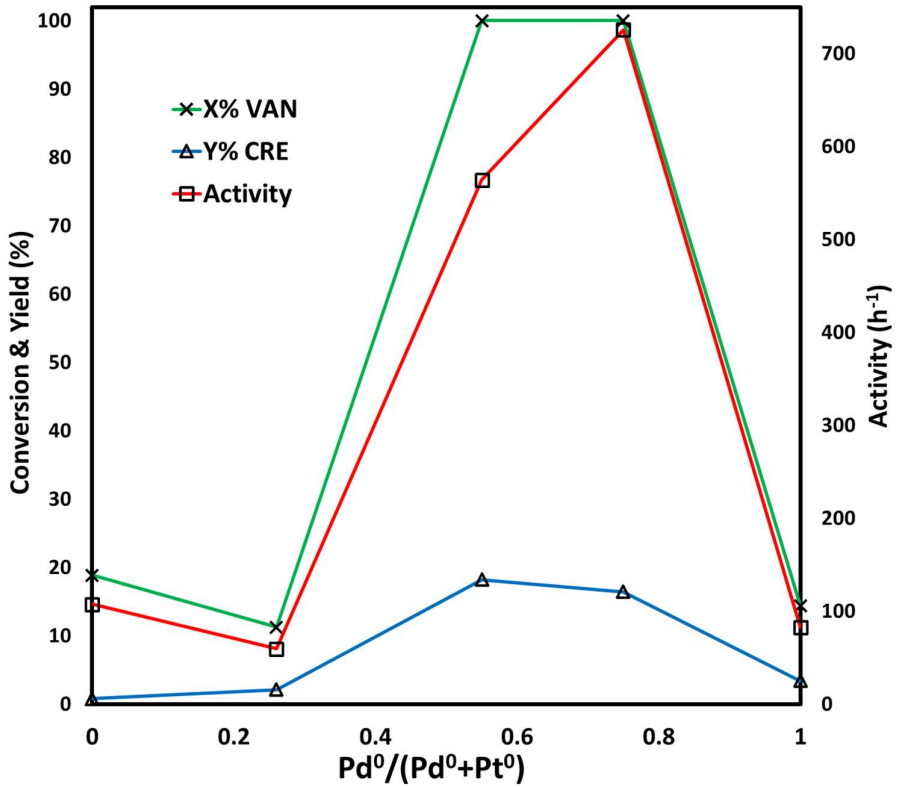

Figure 51. Catalytic performances versus surface $Pd^0/(Pd^0+Pt^0)$ ratio.

A notable observation from the analysis is the presence of a volcano-like correlation (Figure 51), in good correlation with that observed for ICP results. Moreover, the surface metal ratio by XPS correlated to catalytic behaviour demonstrated a narrower region in the Pd^0/ (Pt^0+ Pd^0) value spectrum corresponding to the region identified in the ICP analysis, providing further clues on the optimal compositional conditions of the two metals in order to obtain the best performances.

The Pd^0 to (Pd^0+Pt^0) ratio in bimetallic Pd-Pt catalysts plays a crucial role in influencing the catalytic activity in the hydrodeoxygenation of vanillin. It has been observed that varying the ratio of metallic Pd to the sum of metallic Pd and metallic Pt significantly impacts the catalytic performance in this reaction. Generally, an optimal balance between Pd and Pt content is essential for maximizing catalytic activity in the HDO of vanillin. Specifically, there exists a range of ratios wherein catalytic activity is notably enhanced, leading to more efficient conversion of vanillin to desired products. This optimal ratio, typically observed between specific percentages of Pd weight content relative to the total metal weight, ensures effective hydrogenation and deoxygenation reactions during the HDO process. Beyond this range, deviations in the Pd to (Pd+Pt) ratio results in reduced conversion efficiency and product selectivity.

8 CONCLUSIONS

The study's findings confirm the significant impact of the support, reaction conditions and the synergistic effects of bimetallic catalysts, particularly Pd-Pt combinations, on catalytic performances. The choice of support crucially influences the dispersion and stabilization of Pd particles, directly affecting catalyst activity and selectivity. The introduction of platinum as a second metal in bimetallic catalysts not only enhances catalytic efficiency beyond what is possible with monometallic systems but also allows for greater control over reaction selectivity and efficiency. These findings highlight the significance of the synergy between Pd and Pt within the bimetallic catalyst, leading to enhanced dispersion of active metal species and promotional electronic effects. The presence of Pd and Pt in their metallic state on the catalyst's surface is key to the observed high catalytic activity and selectivity, affirming the effectiveness of the sol-immobilization methodology. Furthermore, the experiments demonstrate how temperature and hydrogen pressure are pivotal in steering the catalytic process, affecting reaction rates, equilibrium shifts, and thereby product distribution, reaching a reaction rate more than 1200 h^{-1} for monometallic Pd/TiO_2 just increasing the temperature at 50°C.

Optimizing the Pd to Pt ratio is crucial for achieving desired catalytic activity and selectivity, significantly influencing catalytic performance. The Pd_3Pt_1 and Pd_1Pt_1 ratios demonstrated superior performance compared to other ratios, highlighting the substantial impact of metal ratios in bimetallic systems on the outcomes of reactions. Additionally, tests on Pd_3Pt_1 at various temperatures and reaction times revealed its ability to convert vanillin nearly completely at just 50°C within 2 hours.

These findings strongly support the notion that hydrodeoxygenation can occur with almost 100% selectivity under very mild conditions.

9 PERSPECTIVES

The results underscored the significant impact of bimetallic ratios on catalytic performance, showcasing the promise of these systems. While our study focused on the active phase rather than support optimization, exploring advanced supports like zeolites combined with metallic oxides could unlock even greater performance.

Another crucial step in the advancement of this material research involves exploring alternative preparation methods. While the sol-immobilization method proves advantageous for small-scale catalyst synthesis, scaling up presents challenges including low reproducibility, higher costs, and waste management concerns. Therefore, investigating methods akin to large-scale production, such as impregnation and precipitation, or innovating new techniques to meet growing production demands, is imperative for bimetallic systems development.

Throughout several chapters of this thesis, model molecules have been extensively discussed to symbolize the actual raw material for lignocellulosic biomass valorisation, which inherently holds greater complexity. Hence, conducting tests on the most effective catalysts directly using bio-oil or pretreated lignocellulosic material is pivotal. This step offers insights into the practical applicability of these catalysts, essential for validating our research findings in real-world biomass conversion applications.

10 BIBLIOGRAPHY

[1] S. Bilgen, Structure and environmental impact of global energy consumption, Renewable and Sustainable Energy Reviews 38 (2014) 890–902. https://doi.org/10.1016/j.rser.2014.07.004.

[2] Energy Institute - Statistical Review of World Energy, Other renewables (including geothermal and biomass), (2023).

[3] J.H. Clark, Green chemistry for the second generation biorefinery - Sustainable chemical manufacturing based on biomass, Journal of Chemical Technology and Biotechnology 82 (2007) 603–609. https://doi.org/10.1002/jctb.1710.

[4] M.W. Seo, S.H. Lee, H. Nam, D. Lee, D. Tokmurzin, S. Wang, Y.K. Park, Recent advances of thermochemical conversieon processes for biorefinery, Bioresour Technol 343 (2022). https://doi.org/10.1016/j.biortech.2021.126109.

[5] E.L. Hrrst, THE CHEMICAL STRUCTURE OF THE HEMICELLULOSES, n.d.

[6] J.N. Nigam, Bioconversion of water-hyacinth (Eichhornia crassipes) hemicellulose acid hydrolysate to motor fuel ethanol by xylose-fermenting yeast, 2002. www.elsevier.com/locate/jbiotec.

[7] J. Zakzeski, P.C.A. Bruijnincx, A.L. Jongerius, B.M. Weckhuysen, The catalytic valorization of lignin for the production of renewable chemicals, Chem Rev 110 (2010) 3552–3599. https://doi.org/10.1021/cr900354u.

[8] N.R. Baral, A. Shah, Comparative techno-economic analysis of steam explosion, dilute sulfuric acid, ammonia fiber explosion and biological pretreatments of corn stover, Bioresour Technol 232 (2017) 331–343. https://doi.org/10.1016/j.biortech.2017.02.068.

[9] P. Kuntke, K.M. Śmiech, H. Bruning, G. Zeeman, M. Saakes, T.H.J.A. Sleutels, H.V.M. Hamelers, C.J.N. Buisman, Ammonium recovery and energy production from urine by a microbial fuel cell, Water Res 46 (2012) 2627–2636. https://doi.org/10.1016/j.watres.2012.02.025.

[10] T.R. Sarker, F. Pattnaik, S. Nanda, A.K. Dalai, V. Meda, S. Naik, Hydrothermal pretreatment technologies for lignocellulosic biomass: A review of steam explosion and subcritical water hydrolysis, Chemosphere 284 (2021). https://doi.org/10.1016/j.chemosphere.2021.131372.

[11] M. Broda, D.J. Yelle, K. Serwańska, Bioethanol Production from Lignocellulosic Biomass—Challenges and Solutions, Molecules 27 (2022). https://doi.org/10.3390/molecules27248717.

[12] L.T. Mika, E. Cséfalvay, Á. Németh, Catalytic Conversion of Carbohydrates to Initial Platform Chemicals: Chemistry and Sustainability, Chem Rev 118 (2018) 505–613. https://doi.org/10.1021/acs.chemrev.7b00395.

[13] A. Deneyer, S. Tlatli, M. Dusselier, B.F. Sels, Branching-First: Synthesizing C-C Skeletal Branched Biobased Chemicals from Sugars, ACS Sustain Chem Eng 6 (2018) 7940–7950. https://doi.org/10.1021/acssuschemeng.8b01234.

[14] J. Zakzeski, P.C.A. Bruijnincx, A.L. Jongerius, B.M. Weckhuysen, The catalytic valorization of lignin for the production of renewable chemicals, Chem Rev 110 (2010) 3552–3599. https://doi.org/10.1021/cr900354u.

[15] A. Molino, S. Chianese, D. Musmarra, Biomass gasification technology: The state of the art overview, Journal of Energy Chemistry 25 (2016) 10–25. https://doi.org/10.1016/j.jechem.2015.11.005.

[16] A. V. Bridgwater, Review of fast pyrolysis of biomass and product upgrading, Biomass Bioenergy 38 (2012) 68–94. https://doi.org/10.1016/j.biombioe.2011.01.048.

[17] D.M. Alonso, S.G. Wettstein, J.A. Dumesic, Bimetallic catalysts for upgrading of biomass to fuels and chemicals, Chem Soc Rev 41 (2012) 8075–8098. https://doi.org/10.1039/c2cs35188a.

[18] C. Liu, H. Wang, A.M. Karim, J. Sun, Y. Wang, Catalytic fast pyrolysis of lignocellulosic biomass, Chem Soc Rev 43 (2014) 7594–7623. https://doi.org/10.1039/c3cs60414d.

[19] J.I. Montoya, C. Valdés, F. Chejne, C.A. Gómez, A. Blanco, G. Marrugo, J. Osorio, E. Castillo, J. Aristóbulo, J. Acero, Bio-oil production from Colombian bagasse by fast pyrolysis in a fluidized bed: An experimental study, J Anal Appl Pyrolysis 112 (2015) 379–387. https://doi.org/10.1016/j.jaap.2014.11.007.

[20] Q. Bu, H. Lei, A.H. Zacher, L. Wang, S. Ren, J. Liang, Y. Wei, Y. Liu, J. Tang, Q. Zhang, R. Ruan, A review of catalytic hydrodeoxygenation of lignin-derived phenols from biomass pyrolysis, Bioresour Technol 124 (2012) 470–477. https://doi.org/10.1016/j.biortech.2012.08.089.

[21] L. Leng, H. Li, X. Yuan, W. Zhou, H. Huang, Bio-oil upgrading by emulsification/microemulsification: A review, Energy 161 (2018) 214–232. https://doi.org/10.1016/j.energy.2018.07.117.

[22] H. Prajitno, R. Insyani, J. Park, C. Ryu, J. Kim, Non-catalytic upgrading of fast pyrolysis bio-oil in supercritical ethanol and combustion behavior of the upgraded oil, Appl Energy 172 (2016) 12–22. https://doi.org/10.1016/j.apenergy.2016.03.093.

[23] J. Wang, Z. Zhong, B. Zhang, K. Ding, Z. Xue, A. Deng, R. Ruan, Upgraded bio-oil production via catalytic fast co-pyrolysis of waste cooking oil and tea residual, Waste Management 60 (2017) 357–362. https://doi.org/10.1016/j.wasman.2016.09.008.

[24] Y. Wang, J. Wu, S. Wang, Hydrodeoxygenation of bio-oil over Pt-based supported catalysts: Importance of mesopores and acidity of the support to compounds with different oxygen contents, RSC Adv 3 (2013) 12635–12640. https://doi.org/10.1039/c3ra41405a.

[25] H. Pourzolfaghar, F. Abnisa, W.M.A. Wan Daud, M.K. Aroua, Atmospheric hydrodeoxygenation of bio-oil oxygenated model compounds: A review, J Anal Appl Pyrolysis 133 (2018) 117–127. https://doi.org/10.1016/j.jaap.2018.04.013.

[26] W. Jin, L. Pastor-Pérez, D.K. Shen, A. Sepúlveda-Escribano, S. Gu, T. Ramirez Reina, Catalytic Upgrading of Biomass Model Compounds: Novel Approaches and Lessons Learnt from Traditional Hydrodeoxygenation – a Review, ChemCatChem 11 (2019) 924–960. https://doi.org/10.1002/cctc.201801722.

[27] X. Wang, M. Arai, Q. Wu, C. Zhang, F. Zhao, Hydrodeoxygenation of lignin-derived phenolics-a review on the active sites of supported metal catalysts, Green Chemistry 22 (2020) 8140–8168. https://doi.org/10.1039/d0gc02610g.

[28] Y. Wu, Y. Sun, K. Liang, Z. Yang, R. Tu, X. Fan, S. Cheng, H. Yu, E. Jiang, X. Xu, Enhancing Hydrodeoxygenation of Bio-oil via Bimetallic Ni-V Catalysts Modified by Cross-Surface Migrated-Carbon from Biochar, ACS Appl Mater Interfaces 13 (2021) 21482–21498. https://doi.org/10.1021/acsami.1c05350.

[29] Z. Li, S. Ji, Y. Liu, X. Cao, S. Tian, Y. Chen, Z. Niu, Y. Li, Well-Defined Materials for Heterogeneous Catalysis: From Nanoparticles to Isolated Single-Atom Sites, Chem Rev 120 (2020) 623–682. https://doi.org/10.1021/acs.chemrev.9b00311.

[30] T.H. Parsell, B.C. Owen, I. Klein, T.M. Jarrell, C.L. Marcum, L.J. Haupert, L.M. Amundson, H.I. Kenttämaa, F. Ribeiro, J.T. Miller, M.M. Abu-Omar, Cleavage and hydrodeoxygenation (HDO) of C-O bonds relevant to lignin conversion using Pd/Zn synergistic catalysis, Chem Sci 4 (2013) 806–813. https://doi.org/10.1039/c2sc21657d.

[31] E. Santillan-Jimenez, M. Perdu, R. Pace, T. Morgan, M. Crocker, Activated carbon, carbon nanofiber and carbon nanotube supported molybdenum carbide catalysts for the hydrodeoxygenation of guaiacol, Catalysts 5 (2015) 424–441. https://doi.org/10.3390/catal5010424.

[32] J.E. Peters, J.R. Carpenter, D.C. Dayton, Anisole and guaiacol hydrodeoxygenation reaction pathways over selected catalysts, Energy and Fuels 29 (2015) 909–916. https://doi.org/10.1021/ef502551p.

[33] M. Liu, J. Zhang, L. Zheng, G. Fan, L. Yang, F. Li, Significant Promotion of Surface Oxygen Vacancies on Bimetallic CoNi Nanocatalysts for Hydrodeoxygenation of Biomass-derived Vanillin to Produce Methylcyclohexanol, ACS Sustain Chem Eng 8 (2020) 6075–6089. https://doi.org/10.1021/acssuschemeng.0c01015.

[34] P. Mäki-Arvela, D.Y. Murzin, Hydrodeoxygenation of lignin-derived phenols: From fundamental studies towards industrial applications, Catalysts 7 (2017). https://doi.org/10.3390/catal7090265.

[35] M. Shetty, K. Murugappan, W.H. Green, Y. Román-Leshkov, Structural Properties and Reactivity Trends of Molybdenum Oxide Catalysts Supported on Zirconia for the Hydrodeoxygenation of Anisole, ACS Sustain Chem Eng 5 (2017) 5293–5301. https://doi.org/10.1021/acssuschemeng.7b00642.

[36] X. Zhang, Q. Zhang, T. Wang, L. Ma, Y. Yu, L. Chen, Hydrodeoxygenation of lignin-derived phenolic compounds to hydrocarbons over Ni/SiO2-ZrO2 catalysts, Bioresour Technol 134 (2013) 73–80. https://doi.org/10.1016/j.biortech.2013.02.039.

[37] H. Ohta, H. Kobayashi, K. Hara, A. Fukuoka, Hydrodeoxygenation of phenols as lignin models under acid-free conditions with carbon-supported platinum catalysts, Chemical Communications 47 (2011) 12209–12211. https://doi.org/10.1039/c1cc14859a.

[38] H. Lee, H. Kim, M.J. Yu, C.H. Ko, J.K. Jeon, J. Jae, S.H. Park, S.C. Jung, Y.K. Park, Catalytic Hydrodeoxygenation of Bio-oil Model Compounds over Pt/HY Catalyst, Sci Rep 6 (2016). https://doi.org/10.1038/srep28765.

[39] S. Jin, Z. Xiao, C. Li, X. Chen, L. Wang, J. Xing, W. Li, C. Liang, Catalytic hydrodeoxygenation of anisole as lignin model compound over supported nickel catalysts, Catal Today 234 (2014) 125–132. https://doi.org/10.1016/j.cattod.2014.02.014.

[40] C.M. Olmos, L.E. Chinchilla, A. Villa, J.J. Delgado, H. Pan, A.B. Hungría, G. Blanco, J.J. Calvino, L. Prati, X. Chen, Influence of pretreatment atmospheres on the performance of bimetallic Au-Pd supported on ceria-zirconia mixed oxide catalysts for benzyl alcohol oxidation, Appl Catal A Gen 525 (2016) 145–157. https://doi.org/10.1016/j.apcata.2016.07.013.

[41] R. Liu, H.M. Chen, L.P. Fang, C. Xu, Z. He, Y. Lai, H. Zhao, D. Bekana, J.F. Liu, Au@Pd Bimetallic Nanocatalyst for Carbon-Halogen Bond Cleavage: An Old Story with New Insight into How the Activity of Pd is Influenced by Au, Environ Sci Technol 52 (2018) 4244–4255. https://doi.org/10.1021/acs.est.7b05996.

[42] P. Wu, D. Zhao, G. Lu, C. Cai, Supported Pd-Au bimetallic nanoparticles as an efficient catalyst for the hydrodeoxygenation of vanillin with formic acid at room temperature, Green Chemistry 24 (2022) 1096–1102. https://doi.org/10.1039/d1gc04240h.

[43] H. Zhang, M. Jin, Y. Xia, Enhancing the catalytic and electrocatalytic properties of Pt-based catalysts by forming bimetallic nanocrystals with Pd, Chem Soc Rev 41 (2012) 8035–8049. https://doi.org/10.1039/c2cs35173k.

[44] Y. Zhai, M. Chu, N. Shang, C. Wang, H. Wang, Y. Gao, Bimetal Co8Ni2 catalyst supported on chitin-derived N-containing carbon for upgrade of biofuels, Appl Surf Sci 506 (2020). https://doi.org/10.1016/j.apsusc.2019.144681.

[45] M. Sankar, N. Dimitratos, P.J. Miedziak, P.P. Wells, C.J. Kiely, G.J. Hutchings, Designing bimetallic catalysts for a green and sustainable future, Chem Soc Rev 41 (2012) 8099–8139. https://doi.org/10.1039/c2cs35296f.

[46] A.R. Ardiyanti, S.A. Khromova, R.H. Venderbosch, V.A. Yakovlev, H.J. Heeres, Catalytic hydrotreatment of fast-pyrolysis oil using non-sulfided bimetallic Ni-Cu catalysts on a δ-Al 2O 3 support, Appl Catal B 117–118 (2012) 105–117. https://doi.org/10.1016/j.apcatb.2011.12.032.

[47] J. Zhong-Yu, T.-Q. Zhang, J.-W. Shang, M.-L. Zhai, Y. Hao, Q. Cong-Zhen, M.A. Xin-Qi, Influence of Cu and Mo components of γ-Al 2 O 3 supported nickel catalysts on hydrodeoxygenation of fatty acid methyl esters to fuel-like hydrocarbons, 2018.

[48] Z. Lv, Q. Sun, X. Meng, F.S. Xiao, Superhydrophilic mesoporous sulfonated melamine-formaldehyde resin supported palladium nanoparticles as an efficient catalyst for biofuel upgrade, J Mater Chem A Mater 1 (2013) 8630–8635. https://doi.org/10.1039/c3ta10916j.

[49] X. Yang, Y. Liang, Y. Cheng, W. Song, X. Wang, Z. Wang, J. Qiu, Hydrodeoxygenation of vanillin over carbon nanotube-supported Ru catalysts assembled at the interfaces of emulsion droplets, Catal Commun 47 (2014) 28–31. https://doi.org/10.1016/j.catcom.2013.12.027.

[50] H. Jiang, X. Yu, X. Peng, H. Zhang, R. Nie, X. Lu, D. Zhou, Q. Xia, Efficient aqueous hydrodeoxygenation of vanillin over a mesoporous carbon nitride-modified Pd nanocatalyst, RSC Adv 6 (2016) 69045–69051. https://doi.org/10.1039/c6ra11851h.

[51] J.L. Santos, M. Alda-Onggar, V. Fedorov, M. Peurla, K. Eränen, P. Mäki-Arvela, M. Centeno, D.Y. Murzin, Hydrodeoxygenation of vanillin over carbon supported metal catalysts, Appl Catal A Gen 561 (2018) 137–149. https://doi.org/10.1016/j.apcata.2018.05.010.

[52] S. Alijani, S. Capelli, C. Evangelisti, L. Prati, A. Villa, S. Cattaneo, Influence of carbon support properties in the hydrodeoxygenation of vanillin as lignin model compound, Catal Today 367 (2021) 220–227. https://doi.org/10.1016/j.cattod.2020.04.026.

[53] P.M. De Souza, R.C. Rabelo-Neto, L.E.P. Borges, G. Jacobs, B.H. Davis, D.E. Resasco, F.B. Noronha, Hydrodeoxygenation of Phenol over Pd Catalysts. Effect of Support on Reaction Mechanism and Catalyst Deactivation, ACS Catal 7 (2017) 2058–2073. https://doi.org/10.1021/acscatal.6b02022.

[54] S. Capelli, S. Cattaneo, M. Stucchi, B.D. Vandegehuchte, A. Chieregato, A. Villa, L. Prati, The Nature of Active Sites in the Pd/C-Catalyzed Hydrogenation/Hydrodeoxygenation of Benzaldehyde, Catalysts 12 (2022). https://doi.org/10.3390/catal12030251.

[55] F. Kawai, X. Hu, Biochemistry of microbial polyvinyl alcohol degradation, Appl Microbiol Biotechnol 84 (2009) 227–237. https://doi.org/10.1007/s00253-009-2113-6.

[56] T.A. El-Brolossy, T. Abdallah, M.B. Mohamed, S. Abdallah, K. Easawi, S. Negm, H. Talaat, Shape and size dependence of the surface plasmon resonance of gold nanoparticles studied by Photoacoustic technique, in: European Physical

Journal: Special Topics, 2008: pp. 361–364. https://doi.org/10.1140/epjst/e2008-00462-0.

[57] E. Aliu, A. Hart, J. Wood, Mild-Temperature hydrodeoxygenation of vanillin a typical bio-oil model compound to Creosol a potential future biofuel, Catal Today 379 (2021) 70–79. https://doi.org/10.1016/j.cattod.2020.05.066.

[58] J. He, C. Zhao, J.A. Lercher, Impact of solvent for individual steps of phenol hydrodeoxygenation with Pd/C and HZSM-5 as catalysts, J Catal 309 (2014) 362–375. https://doi.org/10.1016/j.jcat.2013.09.009.

[59] K. Nakajima, Y. Baba, R. Noma, M. Kitano, J. N. Kondo, S. Hayashi, M. Hara, Nb2O5•nH2O as a heterogeneous catalyst with water-tolerant lewis acid sites, J Am Chem Soc 133 (2011) 4224–4227. https://doi.org/10.1021/ja110482r.

[60] C. Valderrama, X. Gamisans, X. de las Heras, A. Farrán, J.L. Cortina, Sorption kinetics of polycyclic aromatic hydrocarbons removal using granular activated carbon: Intraparticle diffusion coefficients, J Hazard Mater 157 (2008) 386–396. https://doi.org/10.1016/j.jhazmat.2007.12.119.

[61] C.M. Olmos, L.E. Chinchilla, A.M. Cappella, A. Villa, J.J. Delgado, A.B. Hungría, G. Blanco, J.J. Calvino, L. Prati, X. Chen, Selective oxidation of veratryl alcohol over Au-Pd/Ce0.62Zr0.38O2 catalysts synthesized by sol-immobilization: Effect of Au:Pd molar ratio, Nanomaterials 8 (2018). https://doi.org/10.3390/nano8090669.

[62] C. Liu, Z. Shao, Z. Xiao, C.T. Williams, C. Liang, Hydrodeoxygenation of benzofuran over silica-alumina-supported Pt, Pd, and Pt-Pd catalysts, in: Energy and Fuels, 2012: pp. 4205–4211. https://doi.org/10.1021/ef300694c.

[63] T. Li, H. Li, C. Li, Hydrodeoxygenation of vanillin to creosol under mild conditions over carbon nanospheres supported palladium catalysts: Influence of the carbon defects on surface of catalysts, Fuel 310 (2022). https://doi.org/10.1016/j.fuel.2021.122432.

[64] J.X. Tang, Q.S. Chen, L.X. You, H.G. Liao, S.G. Sun, S.G. Zhou, Z.N. Xu, Y.M. Chen, G.C. Guo, Screw-like PdPt nanowires as highly efficient electrocatalysts for methanol and ethylene glycol oxidation, J Mater Chem A Mater 6 (2018) 2327–2336. https://doi.org/10.1039/c7ta09595c.